Potency of all-D amino acid antimicrobial peptides derived from the bovine rumen microbiome on tuberculous and non-tuberculous mycobacteria

Céline Boidin-Wichlacz, Marc Maresca, Isabelle Correia, Olivier Lequin, Vanessa Point, Magali Casanova, Alexis Reinbold, Olga Iranzo, Sharon Huws, Priscille Brodin, et al.

Current Research in Microbial Sciences 8 (2025) 100395

Contents lists available at ScienceDirect

Current Research in Microbial Sciences

journal homepage: www.sciencedirect.com/journal/current-research-in-microbial-sciences

Potency of all-D amino acid antimicrobial peptides derived from the bovine rumen microbiome on tuberculous and non-tuberculous mycobacteria

Céline Boidin-Wichlacz [a], Marc Maresca [b], Isabelle Correia [c], Olivier Lequin [c], Vanessa Point [d], Magali Casanova [d,1], Alexis Reinbold [b], Olga Iranzo [b], Sharon A. Huws [e], Priscille Brodin [a], Linda B. Oyama [e], Aurélie Tasiemski [a], Stéphane Canaan [d], Jean-François Cavalier [d,*]

[a] Univ. Lille, CNRS, INSERM, CHU Lille, Institut Pasteur de Lille, U1019 – UMR9017 - CIIL - Center for Infection and Immunity of Lille, Lille, France
[b] Aix Marseille Univ, CNRS, Centrale Med, ISM2, Marseille, France
[c] Sorbonne Université, Ecole normale supérieure, PSL University, CNRS, Chimie Physique et Chimie du Vivant, CPCV, Paris, France
[d] Aix-Marseille Univ, CNRS, LISM UMR7255, IMM FR3479, Marseille, France
[e] Institute for Global Food Security, School of Biological Sciences, Queen's University Belfast, Belfast BT9 5DL, UK

ARTICLE INFO

Keywords:
Mycobacterial infection
Lynronne
Pore forming activity
Antibiotics
Intracellular activity
Mycobacterium abscessus
Mycobacterium tuberculosis

ABSTRACT

Despite the availability of antibiotics, tuberculosis (TB), caused by *Mycobacterium tuberculosis*, was once again declared the world's leading cause of death from a single infectious agent in 2023. Furthermore, the rising prevalence of drug-resistant strains of *M. tuberculosis*, coupled with the limitations of existing therapeutics, underscores the urgent need for new antimicrobial agents that act through different mechanisms, thereby providing novel therapeutic options. From this perspective, antimicrobial peptides (AMPs) derived from the bovine rumen microbiome have shown promise against many resistant pathogens and may therefore offer a promising alternative against TB. Here, we evaluated the efficacy of AMPs from bovine rumen microbiome, namely the **Lynronne 1, 2** & **3** and **P15s** as well as their **all-D** amino acid enantiomers, against non-tuberculous (*M. abscessus, M. marinum* and *M. smegmatis)* and tuberculous (*M. bovis* BCG, *M. tuberculosis*) mycobacteria. In particular, their antimycobacterial activity was assessed against extracellularly and intracellularly replicating *M. tuberculosis* H37Rv pathogenic strain. Their innocuity was further studied by determining their respective cytotoxicity against human cell lines and hemolytic activity on human erythrocytes. Finally, their mechanism of action was investigated by a membrane permeabilization assay and a lipid insertion assay *via* surface pressure measurement. Although **all-D** enantiomers showed increased cytotoxicity to human cell lines, they still offer a good therapeutic window with improved activity compared to their L-form counterparts, especially **Lynronne 2D$_{all}$** and **P15sD$_{all}$** which emerged as the best growth inhibitors of all mycobacteria. Remarkably, the **all-D** enantiomers also demonstrated activity against intramacrophagic replicating *M. tuberculosis* H37Rv, with very limited toxicity towards human cells and no hemolytic activity at their respective minimum inhibitory concentration. Membrane permeabilization and monolayer lipid insertion assays suggested that these peptides mostly act by insertion into the mycobacterial membrane resulting in a rapid membranolytic effect. These findings highlight the potential of the **all-D** enantiomers of Lynronne peptides, as attractive candidates for the development of new anti-TB drugs. Their effective antibacterial properties combined with low toxicity underscore **Lynronne 2D$_{all}$** and **P15sD$_{all}$** as building blocks for the development of promising alternatives to conventional antibiotics in the treatment of mycobacterial infections, particularly against *M. tuberculosis*.

Abbreviations

AMK	amikacin
AMPs	antimicrobial peptides
CC_{50}	cytotoxic concentration leading to 50 % cell toxicity
CD	circular dichroism
INH	Isoniazid
MDR	multidrug-resistant

* Corresponding author.
E-mail address: jfcavalier@imm.cnrs.fr (J.-F. Cavalier).
[1] Current address: Aix-Marseille Univ, CNRS, INSERM, LAI, Marseille, France

https://doi.org/10.1016/j.crmicr.2025.100395

Available online 22 April 2025

MIC	minimal inhibitory concentration
NTM	nontuberculous mycobacteria
REMA	resazurin microtiter assay
SI_{THP1}	intracellular selectivity index
TB	tuberculosis
TI	therapeutic index

1. Introduction

Despite the widespread availability of antibiotics, tuberculosis (TB) remains a major public health concern with an estimated 10.8 million new cases and nearly 1.25 million deaths in 2023 (WHO, 2024). Although current antibiotic treatments have an impact on both the transmission or outcome of TB, their excessive use also contributes to the emergence of drug-resistant *Mycobacterium tuberculosis* that further undermines TB control programs (WHO, 2024a; 2024b). Rifampicin and isoniazid are essential components of the standard treatment, with a cure rate of about 85–88 % for drug-susceptible TB (Dartois and Dick, 2024, WHO, 2024a). The emergence of multidrug-resistant (MDR) and extensively drug-resistant (XDR) TB has necessitated the exploration of alternative therapeutic approaches to combat this persistent pathogen (WHO, 2024a). However, the six months to more than two years prolonged current treatment regimens strongly contribute to the emergence of antibiotic resistance (Dartois and Dick, 2024, Motta et al., 2024). In 2024, the World Health Organization (WHO) estimated that 400,000 people developed multidrug-resistant or rifampicin-resistant TB with a treatment success rate hovering around 68 % (WHO, 2024a).

In addition to *M. tuberculosis*, nontuberculous mycobacteria (NTM) have gained attention due to their increasing prevalence and the emergence of resistant strains. NTM are opportunistic pathogens responsible for a wide range of bacterial infections, from skin infections caused by *Mycobacterium marinum* (Aubry et al., 2017), to pulmonary infections caused by *Mycobacterium abscessus* (Floto et al., 2016, Griffith et al., 2007, Nessar et al., 2012) especially in immunocompromised people (Leung and Olivier, 2013, Stout et al., 2016). *M. abscessus* exists as two distinct phenotypic morphotypes: a smooth (S) variant associated with biofilm formation and responsible for the primo infection, and an irregular rough (R) variant found in severe and persistent forms of the clinical disease (Catherinot et al., 2007, 2009, Johansen et al., 2020). This mycobacterium is considered one of the most drug-resistant mycobacteria with only a 30–50 % treatment success rate (Candido et al., 2014, Park et al., 2017, Saxena et al., 2021).

The emergence of MDR strains associated with *M. tuberculosis* and/or NTM infections, together with ineffective and expensive therapeutics, poses a significant threat to public health and has paved the way for the development of new antimicrobials that act by different mechanisms and offer new therapeutic options (Dartois and Dick, 2024, Motta et al., 2024, Zhu et al., 2023).

In that context, antimicrobial peptides (AMPs) represent a promising pipeline of natural products with a great potential for clinical use (Ageitos et al., 2017, Gonçalves et al., 2025, Hancock and Sahl, 2006). AMPs derived from various sources have indeed demonstrated interesting antibacterial activities against *M. abscessus* (Bento et al., 2020, Broncano-Lavado et al., 2022, Casanova et al., 2024, da Silva et al., 2020, Iannuzo et al., 2022, Li et al., 2022, Recchia et al., 2023, Sudadech et al., 2021) or *M. tuberculosis* (Abedinzadeh et al., 2015, Degiacomi et al., 2016, Gavrish et al., 2014, Jacobo-Delgado et al., 2023, Mehta et al., 2022, Rao et al., 2021, Rivas-Santiago et al., 2013). Recent studies have highlighted the potential of d-form AMPs, which demonstrate enhanced stability and bioactivity compared to their l-form counterparts, in inhibiting the extracellular and intramacrophage growth of *M. tuberculosis* H37Rv (Lan et al., 2014). The unique mechanisms of action of AMPs, including membrane disruption and immune modulation, position them as valuable candidates for the development of novel therapeutic agents against resistant mycobacterial infections.

As research continues to unlock the potential of AMPs, microbiome-derived peptides could be a game-changer in the ongoing fight against TB and its resistant strains (Jacobo-Delgado et al., 2023, Mehta et al., 2022). Indeed, the bovine rumen microbiome is a complex ecosystem that plays a crucial role in the digestion and fermentation of fibrous plant materials, significantly impacting the health and productivity of ruminants. Among the potential resource for discovering new AMPs, the microbiome of the rumen represents a source of antimicrobials largely underexplored (Chen et al., 2023, Morgavi et al., 2013, Onime et al., 2021, Oyama et al., 2017). Four peptides have been identified from bovine rumen microbiome, namely **Lynronne 1, 2 & 3**, and **P15s** (Mulkern et al., 2022, Oyama et al., 2017). These peptides are believed to have significant implications for the metabolic processes in the rumen and the overall health of the host (Oyama et al., 2017). In addition, they were also found to exhibit significant *in vitro* antibacterial activities against Gram-negative and Gram-positive bacteria including drug-resistant clinical isolates (Mulkern et al., 2022, Oyama et al., 2017). Of interest, topical administration of **Lynronne 1** (10 % *w/v*) to a mouse model of methicillin-resistant *Staphylococcus aureus* (MRSA) wound infection led to a significant (99 %) reduction in bacterial burden ($\geq$ 2-log reduction) (Oyama et al., 2017). In addition, treatment with 32 and 128 mg/kg of **Lynronne 1** & **Lynronne 2**, respectively, provided 100 % protection against *Pseudomonas aeruginosa* PAO1 infection in the *Galleria mellonella* model (Mulkern et al., 2022). Mechanistically, these four AMPs were found to bind bacterial membrane lipids and cause membrane permeabilization both in Gram-negative and Gram-positive bacteria. Although their cytotoxicity against human cells was found minimal (Mulkern et al., 2022, Oyama et al., 2017), their sole limitation, however, is their susceptibility to protease degradation when administered intravenously (Oyama et al., 2017).

Given the promising therapeutic potential of these four rumen microbiome-derived AMPs, this study aimed to evaluate the antimycobacterial activity, innocuity, and mechanism of action of **P15s** and the three **Lynronne** peptides, *i.e.*, **Lynronne 1, 2 & 3**, along with their respective protease-resistant **all-D** amino acid enantiomers against two pathogenic NTM, *M. marinum* and *M. abscessus*; against two tuberculous mycobacteria, *M. bovis* BCG and *M. tuberculosis*; as well as against the closely related saprophytic *M. smegmatis* strain.

2. Experimental section

2.1. Mycobacterial strains, growth conditions and peptides

M. smegmatis mc^2155 strain was grown in Middlebrook 7H9 broth (BD Difco, Le Pont de Claix, France) supplemented with 0.2 % glycerol and 0.05 % Tween 80 (Sigma-Aldrich, St. Quentin Fallavier, France) (7H9-S). *M. abscessus* $CIP104536^T$ with either a smooth (S) or rough (R) morphotype, *M. marinum* ATCC BAA-535/M, *M. bovis* BCG Pasteur 1173P2 and the avirulent *M. tuberculosis* mc^26230 (H37Rv Δ*RD1* Δ*panCD* (Sambandamurthy et al., 2006)) strains were grown in 7H9-S supplemented with 10 % oleic acid, albumin, dextrose, catalase (OADC enrichment; BD Difco) (7H9-S^{OADC}) and 24 μg/mL d-panthothenate (*M. tuberculosis* mc^26230). All cultures were kept at 37 °C, except *M. marinum* which was grown at 32 °C. The pathogenic recombinant strain of *M. tuberculosis* H37Rv expressing an enhanced green fluorescent protein (GFP) (Christophe et al., 2009) was grown at 37 °C for 14 days in 7H9-S^{OADC} supplemented with 50 μg/mL hygromycin B (ThermoFisher Scientific, Illkirch, France).

Lynronne 1 (19 amino acids: LPRRNRWSKIWKKVVTVFS-NH_2), **Lynronne 2** (20 amino acids: HLRRINKLLTRIGLYRHAFG-NH_2), **Lynronne 3** (20 amino acids: NRFTARFRRTPWRLCLQFRQ-NH_2) and **P15s** (20 amino acids: KFVRLKIYCRDKNKGRGISF-NH_2), as well as their **all-D** amino acid enantiomers were obtained from GenScript (Piscataway, NJ, USA) with purity of >95 %. Each peptide was dissolved in sterile water at a stock solution concentration of 10 mg/mL, aliquoted to 100 μL to avoid excessive freezing/thawing, and stored at -20 °C. Sensitivity or resistance to proteolysis of all-L and **all-D** peptides was confirmed using

pepsin, trypsin, and chymotrypsin as previously described (Roblin et al., 2020). Briefly, peptides (5 mg/mL final concentration) were treated with 1 mg/mL (final concentration) pepsin (at pH 2), trypsin or chymotrypsin (at pH 7) (all from Sigma-Aldrich) for 2 h at 37 °C. At the end of the incubation, the proteases were inhibited by the addition of a cell compatible protease inhibitor cocktail (Sigma-Aldrich, P1860). Antimicrobial assay confirmed that the **all-D** peptides, but not their all-L counterparts, were resistant to degradation by the above-mentioned proteases.

2.2. Circular dichroism (CD)

The secondary structure of each peptide was determined by far-UV circular dichroism (CD). CD samples contained ~120 μg/mL peptide concentration in 16 mM sodium phosphate buffer at pH 6.3, in the absence or in the presence of 15 mM SDS. CD spectra were recorded at 25 °C on a Jasco J-815 spectropolarimeter using a quartz cell of 1 mm path length, and were deconvoluted using DichroWeb and SELCON3 analysis method (Whitmore and Wallace, 2004). The deconvolution of d-peptides was performed on the mirror image spectra by inverting the ellipticity sign. The precise concentration of each peptide solution was initially quantified by recording 1D ^{1}H NMR spectra (see **Figures S1-S8** in **Supplementary Material**) on a Bruker Avance III 500 MHz NMR spectrum. See **Supplementary Material** for detailed protocol.

2.3. Minimum inhibitory concentration (MIC) determination via the resazurin microtiter assay

Susceptibility testing was performed using the Middlebrook 7H9 broth microdilution method according to the Clinical and Laboratory Standards Institute (CLSI) guidelines (Woods et al., 2011). All assays for each strain were carried out at least in triplicate. MICs of peptides were determined in sterile 96-well flat-bottom Greiner Bio-One polypropylene microplates with lid (ThermoFisher Scientific), using the REMA assay to better visualize the growth results, as described previously (Blanco-Ruano et al., 2015, Madani et al., 2019, Palomino et al., 2002). The lowest drug concentration inhibiting 50 % and 90 % of growth was defined as the MIC_{50} and MIC_{90}, respectively. See **Supplementary Material** for detailed protocol.

2.4. High-content screening assay in infected macrophages

The intracellular assay was adapted from previous studies (Brodin and Christophe, 2011, Christophe et al., 2010, Christophe et al., 2009, Deboosere et al., 2021, Pethe et al., 2013). The intracellular growth of *M. tuberculosis* H37Rv-GFP was assessed following a 5 days exposure of infected THP-1-derived macrophages (American Type Culture Collection TIB-202) to increasing concentrations of each peptide. To avoid growth of extracellular mycobacteria, cells were extensively washed and treated with amikacin (50 μg/mL) prior to treatment with the AMPs. After 5 days of infection, macrophages were stained with Hoechst 33342 (Life-Technologies), and image acquisition was performed on an automated fluorescence confocal microscope (In Cell analyzer 6000, GE Healthcare) equipped with a 20X (NA 0.70) air lens or 60X (NA 1.2) water lens for the quantification of intracellular *M. tuberculosis* H37Rv-GFP replication. The concentration required to inhibit 50 % of *M. tuberculosis* H37Rv-GFP intracellular growth was defined as the MIC_{50_THP1} (Nguyen et al., 2018, 2017). See **Supplementary Material** for detailed protocol.

2.5. Innocuity of the AMPs: cytotoxic and hemolytic activity

Cytotoxic activity of each peptide was determined using Human bronchial epithelial cells BEAS-2B (ATCC CRL-9609), liver cells HepG2 (ATCC HB-8065), and keratinocyte cells HaCaT (Creative Bioarray, USA) as described previously (Alexander et al., 2024, Casanova et al., 2024). The cytotoxic concentration of peptide leading to 50 % cell death as compared to the control was defined as the CC_{50}. See **Supplementary Material** for detailed protocol.

The hemolytic activity of each peptide was determined as previously described (Mulkern et al., 2022, Oyama et al., 2017, Oyama et al., 2022), from human erythrocytes (red blood cells, *h*RBC; Divbioscience, Ulvenhout, Netherlands) following 1 h incubation at 37 °C, and absorbance reading at $OD_{405\ nm}$ corresponding to hemoglobin release. $DMEM^{FBS}$ and Triton-X100 at 0.1 % (*v/v*) were used as negative (*i.e.*, 0 % hemolysis) and positive (*i.e.*, 100 % hemolysis) controls, respectively. The concentration of peptide leading to 50 % of hemolysis compared to the positive control was defined as the HC_{50}. See **Supplementary Material** for detailed protocol.

2.6. AMP mechanism of action: membrane permeabilization assay and lipid insertion assay through surface pressure measurement

Propidium iodide assay was used to assess *M. tuberculosis* H37Rv membrane permeabilization using 300 μM cetyltrimethylammonium bromide (CTAB, Sigma-Aldrich) as positive control, or 7H9-S^{OADC} alone for the negative control, as described previously (Casanova et al., 2023). Results were expressed in percentage of permeabilization compared to the maximum fluorescence obtained with CTAB, after removing the fluorescence of the negative control. All experiments were done independently at least three times. See **Supplementary Material** for detailed protocol.

Peptide–lipid interaction with total lipid extracts from *M. tuberculosis* was assessed using a reconstituted lipid monolayer at the air-water interface as previously described (Alexander et al., 2024, Casanova et al., 2024, Casanova et al., 2023, Mulkern et al., 2022). The variations in surface pressure due to the insertion of the peptide into the monolayer of total lipids were continuously recorded using a fully automated microtensiometer (μTROUGH SX, Kibron Inc., Helsinki, Finland), in a controlled atmosphere at 20 ± 1 °C (Alexander et al., 2024, Casanova et al., 2024, Casanova et al., 2023, Mulkern et al., 2022). All data were analyzed using the Filmware 2.5 program (Kibron Inc., Helsinki, Finland). See **Supplementary Material** for detailed protocol.

3. Results

3.1. Peptide structural analysis

We previously reported that **Lynronne 1, 2** & **3** possessed at pH 7 a net positive charge of +6, +5 and +6, respectively, with a hydrophobicity ratio of ≥40 % (Oyama et al., 2017). Structural modelling using PEP-FOLD (Shen et al., 2014, Thevenet et al., 2012) showed that the three **Lynronne** peptides would adopt an α-helical conformation of amphipathic nature. NMR spectroscopy of **Lynronne 1** identified a 13-residue amphipathic helix containing all six cationic residues (Jayawant et al., 2021), thereby confirming the overall predicted structure. **P15s** was found to be positively charged (+6) at pH 7 with a hydrophobicity ratio of 35 % and an arginine–lysine (R + K) ratio of 35 % (Mulkern et al., 2022). Similar structural modelling revealed an antiparallel β-sheet turn structure, which is distinct from the α-helical conformations adopted by **Lynronne** peptides (Mulkern et al., 2022).

In the present study, the conformational propensities of the four l-peptides as well as of their **all-D** amino acids enantiomers were investigated by far-UV circular dichroism (CD) (Greenfield, 2006) in aqueous solution and in the presence of SDS detergent as a membrane mimetic (Fig. 1). Far-UV CD works by measuring the absorbance of right- and left-handed polarized light between 180 and 250 nm, thereby revealing secondary structures such as α-helix/β-pleated sheets by analyzing positive and negative peaks (Greenfield, 2006). In fact, α-helical proteins have negative bands at 222 nm and 208 nm, and a positive band at 193 nm (Holzwarth and Doty, 1965); proteins with well-defined antiparallel β-pleated sheets have negative bands near 218 nm and positive

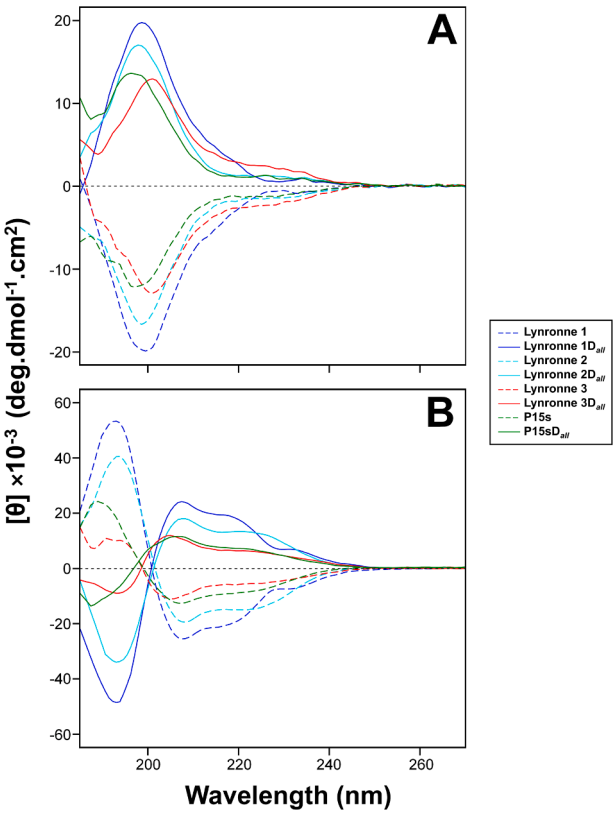

Fig. 1. Circular dichroism (CD) spectra of **Lynronne 1, 2** & **3, P15s** as well as **all-D** enantiomers (120 μg/mL final concentration) in 16 mM sodium phosphate buffer (pH 6.3) in the absence **(A)** or presence **(B)** of 15 mM SDS. Each CD spectrum was collected between 185 and 270 nm and is the average of 4 different scans.

bands at 195 nm (Greenfield and Fasman, 1969), while disordered proteins have very low ellipticity above 210 nm and negative bands near 195 nm (Venyaminov et al., 1993).

The CD data showed that **Lynronne 1, 2** & **3** and **P15s** were mostly unstructured in water, as shown by a negative minimum around 200 nm. Indeed, the deconvolution of their respective CD spectra yielded predominant disordered states, together with a mixture of secondary structures (strand, turn, and helix to a lesser extent) (Fig. 1A and Table 1). Conversely, in the presence of anionic SDS micelles, as previously predicted (Alexander et al., 2024) or determined by NMR for **Lynronne 1** (Jayawant et al., 2021), helical conformations become significantly populated, as evidenced by a characteristic double minimum near 208 and 220 nm. **Lynronne 1** exhibits the highest helical propensity (70 %), followed by **Lynronne 2** (57 %), while **Lynronne 3** and **P15s** have weaker helical propensities (32 % and 22 %, respectively) (Fig. 1B and Table 1). In the case of the **all-D** enantiomers, and as expected for enantiomers, their CD spectra are mirror images of those of the l-peptides (Fig. 1). Consequently, their respective secondary structure populations were found similar to those of the corresponding l-peptide, within ±5 % (Table 1).

Table 1
Secondary structure of **Lynronne 1, 2** & **3** and **P15s** as well as the **all-D** enantiomers in sodium phosphate buffer (pH 6.3) ± SDS micelles, as determined from their respective CD spectra.

Peptides	Condition	% of secondary structures			
		Helix	Strand	Turn	Disordered
Lynronne 1	Buffer	10	31	24	35
	+ SDS	70	2	10	20
Lynronne 2	Buffer	13	22	23	40
	+ SDS	57	8	14	22
Lynronne 3	Buffer	17	29	24	30
	+ SDS	32	24	19	27
P15s	Buffer	8	25	24	43
	+ SDS	22	29	21	31
Lynronne 1D$_{all}$	Buffer	11	23	25	41
	+ SDS	68	1	11	20
Lynronne 2D$_{all}$	Buffer	11	21	24	43
	+ SDS	52	12	16	20
Lynronne 3D$_{all}$	Buffer	15	25	23	32
	+ SDS	28	15	24	27
P15sD$_{all}$	Buffer	7	29	24	40
	+ SDS	28	21	22	29

3.3. Susceptibility testing on selected mycobacteria

The antibacterial properties of the **Lynronne 1** to **3, P15s** and their **all-D** enantiomers were first evaluated against *M. marinum, M. bovis* BCG and *M. abscessus* S & R variants, as well as the saprophytic *M. smegmatis* strain. For each peptide, the corresponding MIC_{50} & MIC_{90} values, as determined by the resazurin microtiter assay (REMA) (Madani et al., 2019, Palomino et al., 2002), are reported in Table 2.

Although **Lynronne 3** and **3D$_{all}$** were found totally inactive (MIC > 1000 μg/mL) against the four mycobacteria tested, variable antibacterial activities were obtained with the other peptides depending on the bacterial strain used. Each active peptide showed comparable MIC_{50} / MIC_{90} values against the non-pathogenic *M. smegmatis* strain (Table 2). With respect to *M. marinum*, this pathogenic strain was unexpectedly highly insensitive to the peptides, with **Lynronne 1** and **P15sD$_{all}$** being the only active growth inhibitors but with moderate to weak MIC_{50} / MIC_{90} values of 39.5 / >1000 and 553 / 916 μg/mL, respectively (Table 2). In contrast, nearly all peptides were active against *M. bovis* BCG and the two variants R & S of *M. abscessus* (Table 2). However, with MIC_{50} & MIC_{90} values ranging from 15.6 to 301 μg/mL and 53.6 to 807 μg/mL, respectively, *M. bovis* BCG was almost 1.2 to up to 15 times more sensitive to these peptides than *M. abscessus* S & R (MIC_{50} ~ 92 to 800 μg/mL; MIC_{90} ~ 264 to >1000 μg/mL). Moreover, in most of the cases, the **all-D** enantiomers were 1.5–6.9 times more active than their respective l-forms (Table 2).

Overall, among the four **all-D** peptides, **Lynronne 2D$_{all}$** and **P15sD$_{all}$** displayed the best MIC_{50} & MIC_{90} values, being the best growth inhibitors of the three mycobacterial species tested, including the two variants S & R of *M. abscessus*.

From these encouraging data obtained on *M. abscessus* and *M. bovis* BCG, drug susceptibility testing of the eight peptides was further assessed using the non-virulent strain *M. tuberculosis* mc^{2}6230 (Sambandamurthy et al., 2006). The best MIC_{50} / MIC_{90} values were observed for **Lynronne 2** (125 / 204 μg/mL), **Lynronne 2D$_{all}$** (62.8 / 114 μg/mL) and **P15sD$_{all}$** (88.2 / 176 μg/mL), with **P15s** being completely inactive (MIC > 1000 μg/mL) (Table 2). While **Lynronne 3** and **3D$_{all}$** remained inactive (MIC_{90} ≥ 1000 μg/mL), surprisingly, **Lynronne 1D$_{all}$** was ~2-times less active than the corresponding **Lynronne 1** L-form.

Overall, *M. tuberculosis* mc^{2}6230 proved to be as sensitive to peptides, especially **Lynronne 2D$_{all}$** and **P15sD$_{all}$**, as *M. bovis* BCG and *M. abscessus*, thus suggesting that these two **all-D** peptides may be promising candidates for further development as anti-TB agents.

3.4. High-content screening assay on virulent M. tuberculosis H37Rv

As previously reported for other classes of potent *M. tuberculosis* growth inhibitors (Nguyen et al., 2018, 2017), the promising MIC values obtained against non-virulent *M. tuberculosis* mc^{2}6230 prompted us to evaluate the antibacterial activity of the eight AMPs against extracellularly- and intracellularly-growing virulent *M. tuberculosis* H37Rv. Antimicrobial activity of the peptides against the extracellular growth of *M. tuberculosis* H37Rv was first monitored after 5 days at 37 °C in the presence of increasing concentrations of peptides.

Table 2
Antibacterial activities (μg/mL) of **Lynronne 1**, **2** & **3**, and **P15s** as well as the **all-D** enantiomers against selected mycobacterial strains [a].

Peptides	MIC_{50} / MIC_{90} (μg/mL)					
	M. tuberculosis mc²6230	*M. bovis* BCG	*M. marinum* M	*M. abscessus* CIP 104536^T		*M. smegmatis* mc²155
				S variant	R variant	
Lynronne 1	246 ± 3.7 / 292 ± 20	40.5 ± 3.5 / >1000	39.5 ± 2.1 / >1000	357 ± 0.7 / 430 ± 37	190 ± 34 / 427 ± 49	33.5 ± 3.8 / 55.4 ± 1.5
Lynronne 2	125 ± 8.1 / 204 ± 6.2	51.5 ± 5.9 / 372 ± 37	>1000	796 ± 78 / >1000	162 ± 2.5 / >1000	76.5 ± 2.4 / 89.1 ± 1.3
Lynronne 3	997 ± 19 / >1000	>1000	>1000	>1000	>1000	>1000
P15s	>1000	301 ± 29 / 807 ± 94	>1000	800 ± 97 / >1000	404 ± 48 / >1000	60.7 ± 0.7 / 65.0 ± 1.9
Lynronne 1D$_{all}$	401 ± 14 / 432 ± 16	>1000	>1000	93 ± 5.9 / 264 ± 18	121 ± 44 / 277 ± 22	15.6 ± 1.2 / 19.0 ± 1.0
Lynronne 2D$_{all}$	62.8 ± 8.1 / 114 ± 11	15.6 ± 0.50 / 53.6 ± 2.1	>1000	147 ± 22 / 335 ± 47	92 ± 14 / 513 ± 45	18.0 ± 1.8 / 18.9 ± 0.9
Lynronne 3D$_{all}$	465 ± 16 / >1000	>1000	>1000	>1000	>1000	>1000
P15sD$_{all}$	88.2 ± 7.2 / 176 ± 13	50.9 ± 1.9 / 129 ± 2.9	553 ± 48 / 916 ± 103	133 ± 10 / 279 ± 41	126 ± 30 / 428 ± 29	20.4 ± 1.7 / 23.5 ± 0.43
INH	0.10 ± 0.012 / 0.15 ± 0.01	0.10 ± 0.01 / 0.24 ± 0.02	2.8 ± 0.10 / 9.2 ± 0.46	>500	>500	3.1 ± 0.06 / 5.6 ± 0.07
RIF	0.01 ± 0.002 / 0.20 ± 0.06	0.02 ± 0.001 / 0.37 ± 0.02	1.2 ± 0.08 / 3.8 ± 0.11	–	–	0.76 ± 0.04 / 2.7 ± 0.19
AMK	0.25 ± 0.015 / 0.37 ± 0.01	0.32 ± 0.02 / 0.48 ± 0.03	0.62 ± 0.03 / 1.7 ± 0.17	2.3 ± 0.11 / 3.4 ± 0.12	4.3 ± 0.15 / 5.9 ± 0.26	–

[a] Experiments were performed as described in the **Methods section**. MIC_{50} / MIC_{90}: peptide minimal concentration leading to 50 % and 90 % inhibition of *in vitro* growth, respectively, as determined by the REMA assay. All values are expressed as mean ± SD ($n \geq 3$) of three independent experiments. INH: isoniazid; RIF: rifampicin; AMK: amikacin.

As a prerequisite for the intracellular assay, the concentration leading to 50 % of THP-1-derived macrophage cell cytotoxicity, *i.e.* CC_{50_THP1}, was determined after 5 days of incubation with each peptide in the absence of infection, prior to performing any intracellular susceptibility testing (Fig. 2A-B). Interestingly, although the all-L peptides exhibited some toxicity after 5 days of incubation, the **all-D** enantiomers were not toxic towards host macrophages with $CC_{50\_THP1} > 1000$ μg/mL, similarly to isoniazid (INH) (Fig. 2A-B and Table 3).

Then, the intracellular growth of *M. tuberculosis* H37Rv-GFP strain was assessed following a 5-day exposure of infected THP-1-derived macrophages to the peptides, using a high-content screening assay based on the fluorescence measurement of GFP-expressing bacteria (Brodin and Christophe 2011, Christophe et al., 2009, Nguyen et al., 2018, Nguyen et al., 2017). In this latter case, the percentage of infected cells, the bacterial area per infected cell, as well as the number of living host cells allowed us to determine the MIC_{50_THP1} of each peptide (Fig. 2 and Table 3), as previously reported in (Christophe et al., 2009, Flipo et al., 2011, Nguyen et al., 2018, 2017). First, *M. tuberculosis* H37Rv-GFP efficiently replicates in THP-1-derived macrophages, as demonstrated by a fold change of 4 at day 5, relative to time 0, in the mean bacterial area per cell (px^2: $pixels^2$), which is directly related to the number of *M. tuberculosis* per cell (Bernard et al., 2020, Queval et al., 2016) (Fig. 2E).

As illustrated in Fig. 2C-D,F-G and summarized in Table 3, some peptides demonstrated antitubercular properties. Regarding the l-peptides, although **Lynronne 3** and **P15s** showed minimal to no activity against the extracellular growth of *M. tuberculosis* H37Rv in culture broth medium, **Lynronne 1** & **2** exhibited moderate MIC_{50} / MIC_{90} values (110 / 189 and 149 / 191 μg/mL, respectively), comparable to those obtained on *M. tuberculosis* mc^26230 (Fig. 2F and Tables 2 & 3). Furthermore, none of these all-l-peptides proved to be active against the intracellular growth of *M. tuberculosis* H37Rv, at concentrations up to their respective CC_{50} values (Fig. 2C and Table 3).

In contrast, the non-toxic **all-D** enantiomers exhibited antibacterial activity against both extracellular and intramacrophagic *M. tuberculosis* H37Rv (Fig. 2D,G and Table 3). Interestingly, **Lynronne 3D$_{all}$** displayed a similar extracellular (MIC_{50} = 138 μg/mL) and intracellular (MIC_{50_THP1} = 182 μg/mL) antibacterial activity. On the other hand, **Lynronne 1D$_{all}$** & **2D$_{all}$** as well as **P15sD$_{all}$** appeared to have a more preferential effect on the extracellular growth of the bacillus, with MIC_{50_THP1} values 3 and up to 16 times higher than their corresponding MIC_{50}s (MIC_{50_THP1} = 483 μg/mL *vs.* MIC_{50} = 69 μg/mL for **Lynronne 1D$_{all}$**; MIC_{50_THP1}= 423 μg/mL *vs.* MIC_{50}= 26 μg/mL for **Lynronne 2D$_{all}$**; and MIC_{50_THP1}= 278 μg/mL *vs.* MIC_{50}= 92 μg/mL for **P15sD$_{all}$**).

These results are best illustrated by the determination of the intracellular selectivity index values, SI_{THP1}, defined here as the ratio of the cytotoxic concentration to its effective intracellular bioactive concentration (*i.e.*, $\frac{CC_{50\_THP1}}{MIC_{50\_THP1}}$). Indeed, with SI_{THP1} values ranging from 2.1 and up to 5.5, the **all-D** enantiomers showed improved activity against intracellular *M. tuberculosis* H37Rv while minimizing toxicity to host macrophage cells, and therefore represent prospective antitubercular derivatives. Such findings therefore highlight the potential of the **all-D** peptides over their all-L counterparts as more effective therapeutic candidates in targeting intracellular *M. tuberculosis* (Table 3).

3.5. Innocuity testing

The innocuity of the different peptides was further evaluated using i) a hemolysis assay with human red blood cells and ii) a resazurin-based cell toxicity assay conducted on human cells from lung (BEAS-2B cells), liver (HepG2), or skin (HaCaT) (Alexander et al., 2024, Foo et al., 2018) (Table 4). The comparison of different cell lines is crucial as it allows us to evaluate the safety and efficacy of the peptides in different biological contexts, which can lead to a better understanding of their potential therapeutic applications and expected outcomes *in vivo*. In good

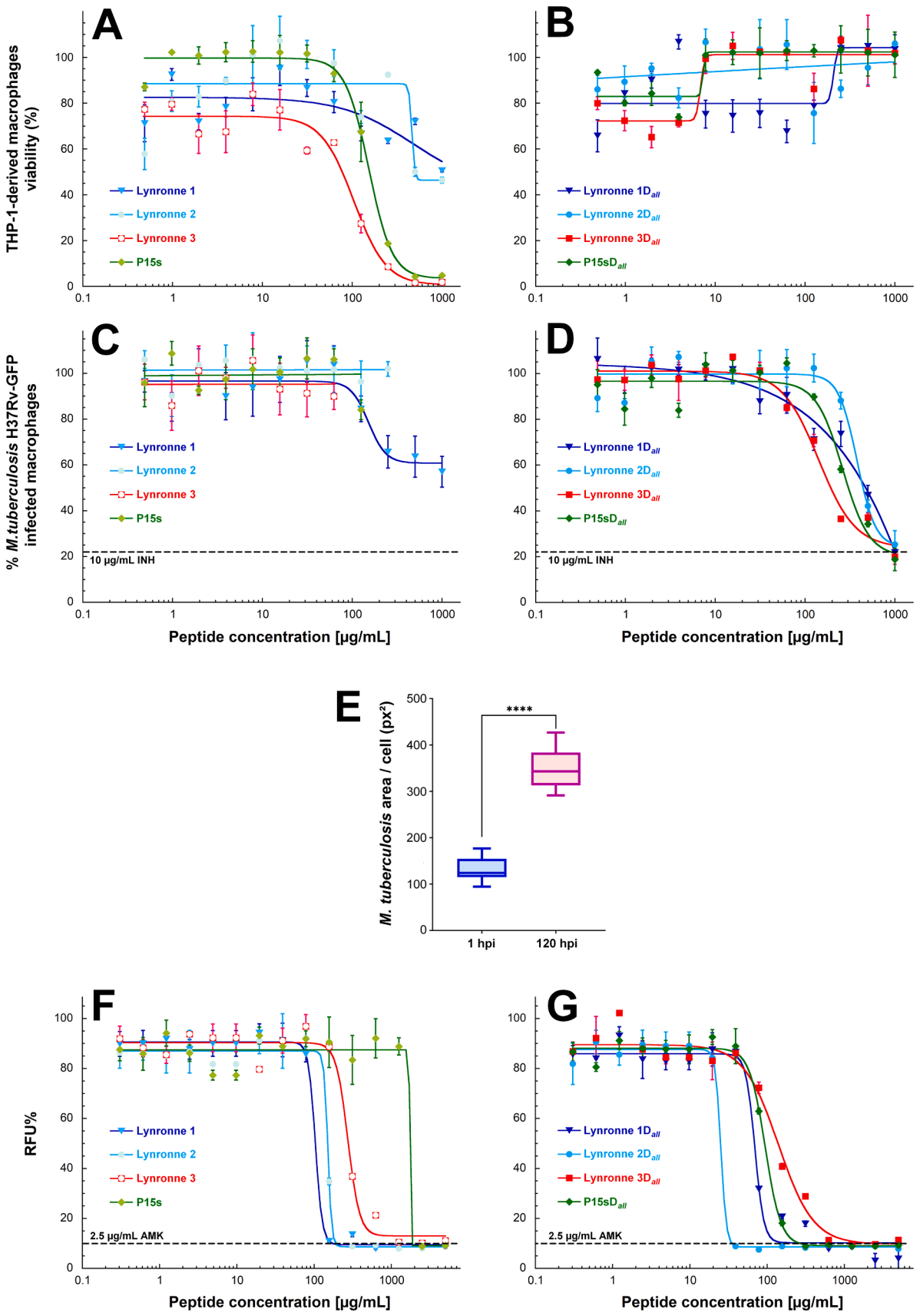

(caption on next page)

Fig. 2. Dose-response activity of the peptides against THP-1-derived macrophages, extracellular and intracellular growth of *M. tuberculosis* H37Rv. (**A-B**) Cytotoxic activity of **Lynronne 1, 2** & **3** and **P15s** (**A**), as well as the **all-D** enantiomers (**B**) on THP-1-derived macrophages. Following 5-day exposure to increasing concentrations of peptides, nuclei were stained with Hoechst 33,342 dye and counted by fluorescence imaging. Results are expressed as normalized relative macrophages viability (%), and are mean ± SD ($n \geq 3$) of three independent experiments. (**C-D**) Intracellular activity of **Lynronne 1, 2** & **3** and **P15s** (**C**), as well as the **all-D** enantiomers (**D**) against GFP-expressing *M. tuberculosis* H37Rv replicating inside THP-1-derived macrophages. Results are expressed as the percentage of infected macrophages after 5 days of infection. The dashed line represents the level of inhibition (~79 %) reached with 10 μg/mL isoniazid (INH), used as control. All values are expressed as mean ± SD ($n \geq 3$) of three independent experiments. (**E**) Box plots showing the *M. tuberculosis* bacterial area (px^2: $pixels^2$) per infected THP-1-derived macrophages at time 0 (*i.e.*, 1 h post-infection) and at day 5 (*i.e.*, 120 h post-infection), which directly correlates with the number of *M. tuberculosis* per infected cell. Results are mean ± SD of three independent experiments. Statistical analysis was done using a non-parametric Mann–Whitney test using Prism 8.0 (Graphpad Inc.): **** p-value < 0.0001. (**F-G**) Activity of **Lynronne 1, 2** & **3** and **P15s** (**F**), as well as the **all-D** enantiomers (**G**) against extracellular *M. tuberculosis* H37Rv replicating in broth medium, using the REMA assay. Results are expressed as normalized relative fluorescence units (RFU %). The dashed line represents the level of inhibition (~90 %) reached with 2.5 μg/mL amikacin (AMK) used as control.

Table 3
Antitubercular activities of **Lynronne 1, 2** & **3**, and **P15s** as well as the **all-D** enantiomers against *M. tuberculosis* H37Rv.

Peptides	Extracellular growth[a]	Intracellular macrophage growth[b]		SI_{THP1}[c]
	MIC_{50} / MIC_{90} (μg/mL)	MIC_{50_THP1} (μg/mL)	CC_{50_THP1} (μg/mL)	
Lynronne 1	110 ± 3.2 / 189 ± 8.2	>1000	>1000	–
Lynronne 2	149 ± 0.5 / 191 ± 3.1	>500	500 ± 8	<1.0
Lynronne 3	277 ± 4.9 / >1000	>77	77 ± 6	<1.0
P15s	>1000	>155	155 ± 9	<1.0
Lynronne 1D$_{all}$	69 ± 2.5 / 174 ± 15	483 ± 26	>1000	>2.1
Lynronne 2D$_{all}$	26 ± 3.1 / 32 ± 3.7	423 ± 27	>1000	>2.4
Lynronne 3D$_{all}$	138 ± 1.4 / >1000	182 ± 9.6	>1000	>5.5
P15sD$_{all}$	92 ± 15 / 289 ± 47	278 ± 18	>1000	>3.6
INH	0.56 ± 0.03 / 0.81 ± 0.005	0.58 ± 0.01	>1000[d]	>172
RIF	0.06 ± 0.002 / 0.12 ± 0.003	0.02 ± 0.001	20[d]	1000
AMK	1.2 ± 0.1 / 3.3 ± 0.25	–	–	–

[a] Experiments were performed as described in the **Methods section**. MIC_{50} / MIC_{90}: peptide minimal concentration leading to 50 % and 90 % inhibition of *in vitro* growth, respectively, as determined by the REMA assay.

[b] MIC_{50_THP1}: minimal compound concentration leading to a 50 % decrease in *M. tuberculosis* H37Rv-GFP growth inside infected macrophages as compared to untreated cells. CC_{50_THP1}: peptide concentration leading to 50 % THP-1 cell cytotoxicity after 5 days of incubation. THP-1-derived macrophages were infected by *M. tuberculosis* H37Rv-GFP at a MOI of 1:1 and intracellular growth was recorded at day 5.

[c] SI_{THP1}, intracellular selectivity index calculated by dividing the CC_{50_THP1} by the MIC_{50_THP1} reached for *M. tuberculosis* H37Rv.

[d] Data from Christophe et al. (2009). All values are expressed as mean ± SD ($n \geq 3$) of three independent experiments. INH, isoniazid; RIF: rifampicin; AMK, amikacin.

Table 4
Evaluation of the innocuity of **Lynronne 1, 2** & **3**, and **P15s** as well as the **all-D** enantiomers towards human cells from lung (BEAS-2B cells), liver (HepG2), or skin (HaCaT), as well as towards red blood cells.

Peptides	CC_{50} (μg/mL)[a]			HC_{50}[b]	Toxicity range	TI[c] range
	BEAS-2B	HepG2	HaCaT	(μg/mL)		
Lynronne 1	179 ± 16	665 ± 30	271 ± 19	594 ± 24	179–665	1.6–6.0
Lynronne 2	850 ± 35	>1000	880 ± 31	>1000	850->1000	5.7->6.7
Lynronne 3	693 ± 27	>1000	>1000	>1000	693->1000	2.5->3.6
P15s	>1000	>1000	>1000	>1000	>1000	–
Lynronne 1D$_{all}$	188 ± 10	477 ± 21	229 ± 20	>1000	188->1000	2.7->14.5
Lynronne 2D$_{all}$	343 ± 18	645 ± 48	279 ± 13	>1000	279->1000	10.7->38.5
Lynronne 3D$_{all}$	877 ± 59	>1000	850 ± 53	>1000	850->1000	6.2->7.2
P15sD$_{all}$	926 ± 51	>1000	955 ± 29	>1000	926->1000	10.1->10.9

[a] Experiments were performed as described in the **Methods section**. CC_{50}: cytotoxic concentration of peptide leading to 50 % cell death *in vitro*, compared to the untreated control.

[b] HC_{50}: hemolytic concentration of peptide leading to 50 % hemolysis *in vitro*, compared to the control.

[c] TI: therapeutic index calculated by dividing the range of CC_{50} or HC_{50} obtained on human cells by the MIC_{50} reached for the extracellular growth of *M. tuberculosis* H37Rv (see Table 3). All values are expressed as mean ± SD (n = 3).

agreement with previous work on the L-peptides (Alexander et al., 2024, Mulkern et al., 2022, Oyama et al., 2017), while **P15s** did not cause toxicity on human cells (CC_{50} > 1000 μg/mL), **Lynronne 1, 2** & **3** demonstrated limited toxicity with CC_{50} values ranging from 179 to 665 μg/mL, from 850 to >1000 μg/mL, and from 693 to >1000 μg/mL, respectively (Table 4 and Fig. 3A,C,E,G). Moreover, the obtained results indicate that while **Lynronne 1** exhibited a notable hemolytic activity with HC_{50} ~ 594 μg/mL, all other peptides, including **Lynronne 2** & **3, P15s** and their **all-D** enantiomers, demonstrated no significant HC_{50} value (> 1000 μg/mL) (Table 4 and Fig. 3G,H). Calculation of their respective therapeutic index (Begg et al., 2001) (TI); *i.e.*, the ratio between CC_{50} or HC_{50} and MIC_{50} on extracellular growth of *M. tuberculosis* H37Rv, resulted in moderate (1.6 to > 6.7) TI values synonymous with a medium-sized window between efficacy and toxicity (Table 4).

Regarding the **all-D** enantiomers, **P15sD$_{all}$** was found to be almost non-toxic like its l-form. In addition, similar toxicity ranges were obtained between the l- and d-forms of **Lynronne 1** & **3**. Conversely, **Lynronne 2D$_{all}$** was almost 2.5–3 times more toxic than its L-

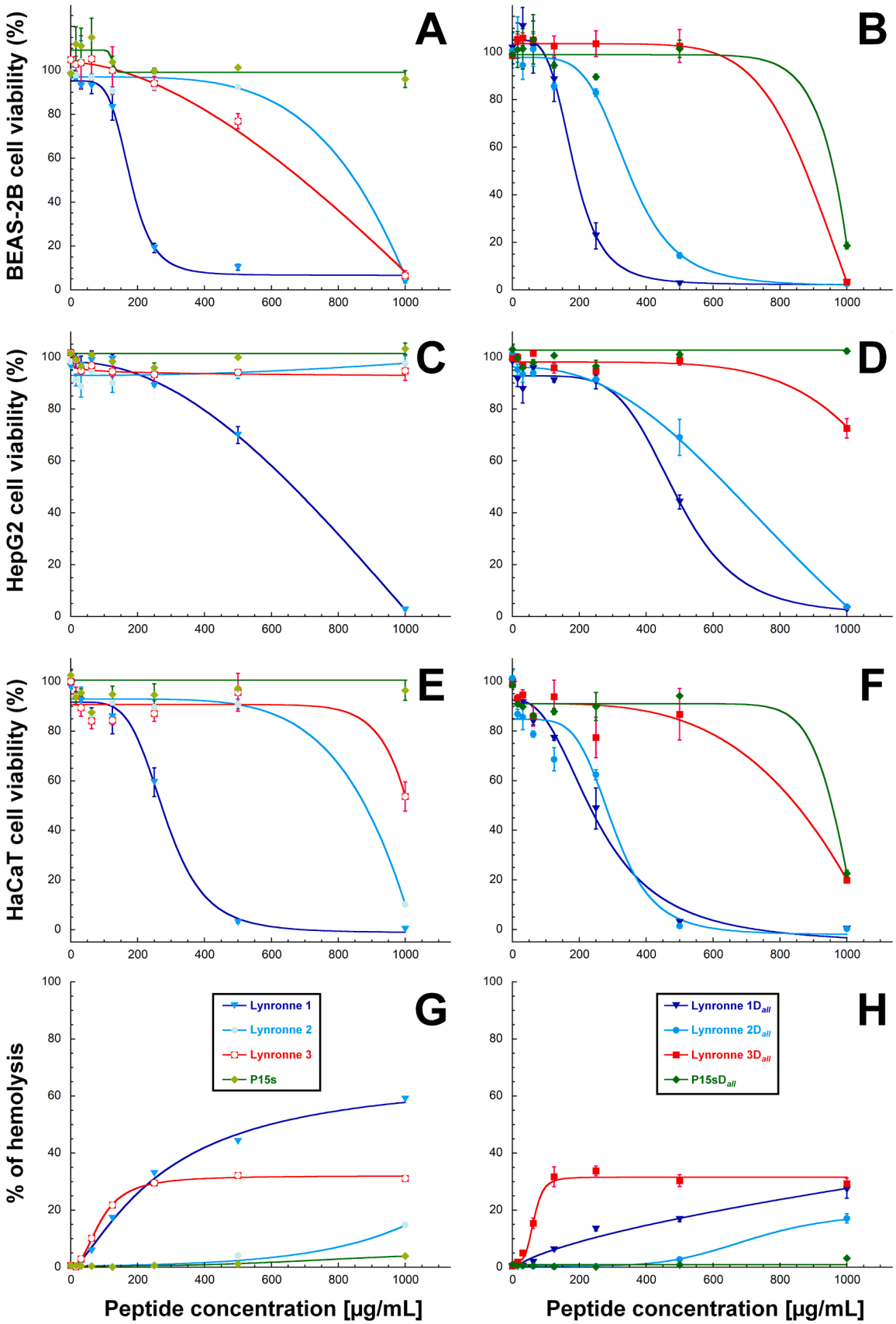

Fig. 3. Cytotoxic and hemolytic activity of Lynronne 1, 2 & 3 and P15s (A,C,E,G) as well as their all-D enantiomers. (B,D,F,H) Cytotoxicity dose-response curves following 48 h-exposure to increasing concentrations of each peptide on human **(A-B)** BEAS-2B (lung), **(C-D)** HepG2 (liver), and **(E-F)** HaCaT (skin) cells, using resazurin assay. **(G-H)** Dose-response curves for human erythrocyte hemolysis after exposure to increasing concentrations of each peptide. Human red blood cells (*h*RBC) were exposed for 1 h before measurement of hemoglobin release. Results are expressed as the mean ± SD of three independent experiments.

enantiomer with CC_{50} values ranging from 279 to 645 μg/mL (Fig. 3B,D, F,H and Table 4).

The apparent selective toxicity of the **all-D** peptides to BEAS-2B, HepG2 and HaCat cells, but not to THP-1-derived macrophages, may be due to differences in cellular defense mechanisms and membrane composition. THP-1-derived macrophages possess sophisticated intracellular protective systems, including membrane damage repair pathways and adaptive responses to antimicrobial peptides (Zanetti, 2004); together with a more robust and cholesterol-rich plasma membrane than epithelial and liver cells, which limits insertion and disruption by antimicrobial peptides (Wimley and Hristova, 2011). In contrast, due to their reduced ability to regulate oxidative stress and membrane permeabilization, epithelial and liver cells are usually more susceptible to antimicrobial peptides (Ma et al., 2024). Moreover, the membrane of BEAS-2B, HepG2 and HaCaT cells is more permeable (Wimley and Hristova, 2011). This may facilitate interaction with the **all-D** peptides, resulting in more pronounced membrane disruption and consequently increased toxicity.

Overall, these results highlight the varying toxicity profiles of the **Lynronne** peptides and their **all-D** enantiomers, indicating that while some derivatives exhibit increased toxicity, **P15sD$_{all}$** remains a promising candidate with minimal cytotoxic effects across the tested cell lines. Considering the MIC_{50} values of **all-D** enantiomers against the extracellular growth of *M. tuberculosis* H37Rv (Table 3), these toxicity ranges therefore translate into therapeutic index (TI) values of 2.7 to >14.5 for **Lynronne 1D$_{all}$**, 10.7 to >38.5 for **Lynronne 2D$_{all}$**, 6.2 to >7.2 for **Lynronne 3D$_{all}$**, and 10.1 to >10.9 for **P15sD$_{all}$**. Given that a drug is generally considered to have a good safety profile when its TI is greater than 10 (Begg et al., 2001, Tamargo et al., 2015), the **all-D** enantiomers therefore present very interesting profiles in terms of toxicity/antibacterial activity ratio, particularly **Lynronne 2D$_{all}$** and **P15sD$_{all}$**.

Overall, the obtained extracellular and intracellular antibacterial activities, together with the low hemolytic and negligible cytotoxic activities against human cell lines indicated that amongst the 8 tested peptides, **Lynronne 1D$_{all}$**, **Lynronne 2D$_{all}$**, and **P15sD$_{all}$** possessed the best combination of antibacterial and innocuity/safety properties. In particular, **P15sD$_{all}$** displayed the highest antibacterial activity against all mycobacterial species tested, along with the lowest toxicity to human cells. Given all these findings, the latter three **all-D** peptides were selected for further investigations.

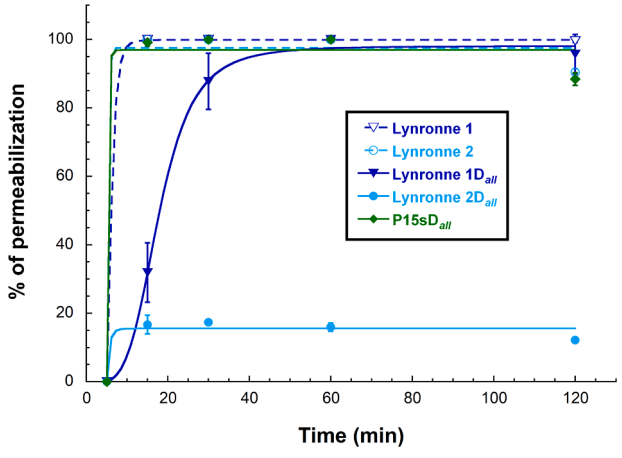

Fig. 4. Effect of Lynronne 1 & 2, their respective all-D enantiomers as well as P15sD$_{all}$ on *M. tuberculosis* H37Rv membrane integrity. *M. tuberculosis* H37Rv was exposed to each peptide at 4 × MIC_{90} concentration. The effect of each peptide on the integrity of the mycobacterial membrane was followed over 120 min, starting at t = 5 min, using propidium iodide, and compared to the maximum fluorescence obtained with 300 μM CTAB (used as positive control giving 100 % permeabilization). Results are expressed as mean ± SD of three independent experiments.

3.6. Mechanism of action

Previous studies have demonstrated that whereas **Lynronne 1** is able to permeabilize the cell membrane of Gram-positive *S. aureus* MRSA USA300 (Oyama et al., 2017) as well as Gram-negative *Acinetobacter baumannii* DSM 30007 (Alexander et al., 2024) and *P. aeruginosa* PAO1 (Mulkern et al., 2022), **Lynronne 2** is only able to permeabilize *P. aeruginosa* PAO1 membrane (Mulkern et al., 2022).

Since mycobacterial membrane strongly differs from that of Gram-positive and Gram-negative bacteria, we thus evaluated the permeabilization effect of **Lynronne 1, 1D$_{all}$, 2** & **2D$_{all}$** and **P15sD$_{all}$** on *M. tuberculosis* H37Rv using propidium iodide as a fluorescence-based dye to evaluate membrane integrity (Fig. 4). The membranolytic detergent cetyltrimethylammonium bromide (CTAB) was used as a positive control, leading to 100 % membrane permeabilization (Iannuzo et al., 2022).

First, **Lynronne 1** & **2** showed quick bacterial membrane permeabilization capabilities reaching 100 % permeabilization of *M. tuberculosis* H37Rv membrane after 15 min of exposure. Although **Lynronne 1D$_{all}$** and **P15sD$_{all}$** were also able to strongly permeabilize the *M. tuberculosis* H37Rv membrane, very little permeabilization activity (~ 16 %) was however observed for **Lynronne 2D$_{all}$** over 120 min. These results suggest that while the antimicrobial activity of **Lynronne 1, 2** & **1D$_{all}$** and **P15sD$_{all}$** result from pore formation, the mechanism of action of **Lynronne 2D$_{all}$** against *M. tuberculosis* is different.

3.7. Peptide interaction with monolayer of total lipid extracts from *M. tuberculosis*

Lynronne 2 and **P15s** were previously reported to interact with lipid monolayers composed of pure 1-palmitoyl-2-oleoyl-*sn*-glycero-3-(phospho-*rac*-(1′-glycerol)) (POPG), cardiolipin (CL), lipoteichoic acid (LTA), or 1-palmitoyl-2-oleoyl-glycero-3-phosphocholine (POPC) (Alexander et al., 2024, Mulkern et al., 2022, Oyama et al., 2017). In contrast, **Lynronne 1** exhibited a clear affinity for anionic PG & CL headgroups that would form favorable interactions with positively charged residues in the peptide sequence, resulting in rapid lysis of model membranes (Alexander et al., 2024, Jayawant et al., 2021, Oyama et al., 2017).

From these findings and given the ability of these peptides to cause membrane permeabilization in *M. tuberculosis*, their ability to insert into monolayer of total lipid extracts from this bacterium was assessed (Fig. 5).

The influence of the initial surface pressure Π_i (Benarouche et al., 2013) on the insertion process of **Lynronne 1** & **2, 1D$_{all}$** & **2D$_{all}$**, and **P15sD$_{all}$** into a monolayer of total lipid extracts from *M. tuberculosis* was first investigated. The plot of the maximal increase in surface pressure ($\Delta\Pi_{max}$) as a function of Π_i (Fig. 5A) allowed us to determine the binding parameters of each peptide for the monolayer (Fig. 5B). First, extrapolation of the linear regression of the plot to the *x* axis provided the critical surface pressure (Π_c) (Calvez et al., 2009, Liu et al., 2022) (Fig. 5A). Π_c is indeed the maximum surface pressure of the monolayer at which peptide insertion is energetically favorable. In fact, this value corresponds to the surface pressure up to which the peptide can insert into the monolayer, and beyond which no insertion takes place. The synergy factor (slope of the linear regression +1), which has been demonstrated to describe peptide/protein affinity for a given lipid monolayer, as well as the $\Delta\Pi_0$ obtained by extrapolating the regression to the *y* axis (*i.e.*, Π_i= 0) (Benarouche et al., 2013, Boisselier et al., 2012, Calvez et al., 2009, Calvez et al., 2011) are also deduced from the same plot (Fig. 5). As defined by the Salesse group (Boisselier et al., 2012, Calvez et al., 2009, Calvez et al., 2011), the observed positive synergy values (0.58–0.74) and the occurrence of a $\Delta\Pi_0$ value (14.0–19.2 mN/m) lower than the corresponding Π_c (39.7–68.4 mN/m) are

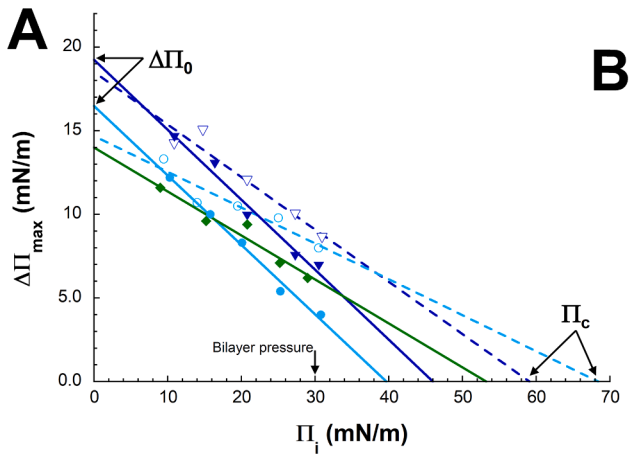

B

Peptides	Linear regression	$\Delta\Pi_0$ (mN/m)	Π_c (mN/m)	Synergy (= slope + 1)
Lynronne 1	y = 18.516 – 0.31309x R² = 0.92771	18.5	59.1	0.687
Lynronne 1D$_{all}$	y = 19.236 – 0.41813x R² = 0.97622	19.2	46.0	0.582
Lynronne 2	y = 14.691 – 0.21475x R² = 0.88785	14.7	68.4	0.785
Lynronne 2D$_{all}$	y = 16.475 – 0.41519x R² = 0.98966	16.5	39.7	0.585
P15sD$_{all}$	y = 13.997 – 0.26294x R² = 0.94457	14.0	53.2	0.737

Fig. 5. Determination of the binding parameters of Lynronne 1 & 2, their respective all-D enantiomers as well as P15sD$_{all}$ into a monomolecular film of total lipid extracts from *M. tuberculosis* mc^{2}6230. Lipid monolayers were obtained by spreading total lipids extracted from *M. tuberculosis* mc^{2}6230 at the air-water interface until the desired initial surface pressure, Π_i= 10 to 30 mN/m, was reached. The peptide (100 μg/mL final concentration) was injected in the aqueous phase below the monomolecular film at various initial Π_i. **(A)** The maximum increase in surface pressure ($\Delta\Pi_{max}$) was recorded using the Langmuir film balance (KIBRON apparatus), and $\Delta\Pi_{max}$ was plotted as a function of Π_i. **(B)** The critical surface pressure for penetration (Π_c; intercept of the linear regression with the *x*-axis), $\Delta\Pi_0$ (intercept of the linear regression with the *y* axis), and the synergy factor (slope of the linear regression +1) were determined.

consistent with the existence of strong peptide-lipid interactions. This was also supported by Πc values above the estimated membrane lateral pressure (30 mN/m) (Marsh 1996), that are indicative of peptide insertion into the monolayer of total lipids from *M. tuberculosis* (Boisselier et al., 2012, Calvez et al., 2009).

In addition, the increase in surface pressure at 30 mN/m revealed a higher insertion ability of **Lynronne 1** (9.12 mN/m), **Lynronne 2** (8.25 mN/m), **Lynronne 1D$_{all}$** (6.70 mN/m), and **P15sD$_{all}$** (6.11 mN/m) compared to **Lynronne 2D$_{all}$** (4.02 mN/m) (Fig. 5A). Notably, the lower insertion of **Lynronne 2D$_{all}$** into lipids correlates well with the previous results obtained for bacterial membrane permeabilization (Fig. 4). The findings from both the mechanism of action studies and the interactions of peptides with lipid monolayers extracted from *M. tuberculosis* highlight the distinct permeabilization capabilities of **Lynronne 2** vs. **Lynronne 2D$_{all}$**. The fact that this latter d-peptide may operate through a different mechanism underscores the importance of better understanding peptide-lipid interactions to optimize the antimicrobial efficacy of AMPs against complex and highly hydrophobic mycobacterial membranes.

4. Discussion

TB remains a significant global health challenge, exacerbated by the emergence of multidrug-resistant (MDR) and extensively drug-resistant (XDR) strains of *M. tuberculosis* (WHO, 2024). The limitations of current antibiotic therapies, which often lead to resistance, necessitate the exploration of alternative treatment strategies.

In this study, we have evaluated the antimycobacterial activity of previously identified antimicrobial peptides from the bovine rumen microbiome, specifically **Lynronne 1, 2 & 3** as well as **P15s** (Oyama et al., 2017). Our goal was to evaluate their efficacy and potency against the growth of pathogenic mycobacteria; including two NTM, *M. marinum* and *M. abscessus*, and two tuberculous mycobacteria, *M. bovis* BCG and *M. tuberculosis*; to determine if these peptides could be promising candidates for the treatment of mycobacteria-associated infections. Moreover, given that previous research had demonstrated that modifications of AMPs, such as the substitution of d-amino acids, could lead to reduce cytotoxicity (Jia et al., 2017), we also evaluated the antimycobacterial activity of their respective **all-D** enantiomers, namely **Lynronne 1D$_{all}$, 2D$_{all}$, 3D$_{all}$** and **P15sD$_{all}$**.

Amino acid sequence analysis of these peptides revealed that they possess a net positive charge and a significant hydrophobicity ratio, which are critical for their interaction with bacterial membranes. Structural examination using circular dichroism indicates that in the presence of anionic SDS micelles, **Lynronne 1, 2 & 3**, and **P15s** demonstrated α-helical conformation based on the observed double minimum peaks near 208 and 220 nm (Greenfield, 2006), thus suggesting that these peptides can effectively insert inside bacterial membranes and disrupt them, a mechanism that is crucial for their antibacterial activity. However, the difference in peak height of the CD spectra indicates that **Lynronne 3** and **P15s** in SDS detergent exhibit only half of the α-helical propensity of **Lynronne 1** or **2** (Table 1). The same structural feature can also be deduced for the **all-D** enantiomers, since their CD spectra are mirrored to those of the l-peptides.

Among the eight peptides evaluated, we demonstrated that the **all-D** enantiomers were overall 1.5 to 6.9 times more active than their respective l-forms (Fig. 2 and Table 3). Of major interest, these four **all-D** enantiomers were also active against the intracellular growth of *M. tuberculosis* H37Rv inside infected macrophages (Fig. 2 and Table 3). Unexpectedly, this set of four peptides can be divided into two classes. Specifically, **Lynronne 3D$_{all}$** showed similar extracellular and intracellular antibacterial activity. In contrast, **Lynronne 1D$_{all}$ & 2D$_{all}$** as well as **P15sD$_{all}$** showed higher activity against extracellular replicating *M. tuberculosis* mycobacteria (Table 3). The observed differences between the intracellular and extracellular inhibition of *M. tuberculosis* growth by the **all-D** enantiomers may probably result from several factors, such as their bioavailability, hydrophobicity, penetration and fate inside the bacteria and/or the infected macrophages. From these results, **Lynronne 2D$_{all}$** and **P15sD$_{all}$** possessed the best combination of antimycobacterial activity against all mycobacteria tested (Fig. 2 and Tables 2 & 3), especially against *M. abscessus* S & R morphotypes and *M. tuberculosis* H37Rv; and cytotoxicity on human macrophages, resulting in relatively good selectivity indexes (Table 3).

Lynronne 1 & 3 have been previously reported to act *via* membrane disruption against Gram-positive *S. aureus* MRSA USA300 (Oyama et al., 2017) as well as Gram-negative *A. baumannii* DSM 30007 (Alexander et al., 2024) and *P. aeruginosa* PAO1 (Mulkern et al., 2022), while **Lynronne 2** was only able to permeabilize *P. aeruginosa* PAO1 membrane (Mulkern et al., 2022). Here, we demonstrated that **Lynronne 1D$_{all}$** and **P15sD$_{all}$** strongly permeabilize *M. tuberculosis* H37Rv membrane, whereas **Lynronne 2D$_{all}$** was noticeably less membrane-destabilizing with only 16 % permeabilization within two hours (Fig. 4). These findings were complemented by the lipid interaction assays carried out on total lipid extracts from *M. tuberculosis*, in

which **Lynronne 1D$_{all}$** and **P15sD$_{all}$** both showed a higher affinity for lipid binding than **Lynronne 2D$_{all}$** (Fig. 5). Taken together, these observations confirm that while **Lynronne 1D$_{all}$** and **P15sD$_{all}$** are effective membrane-disrupting peptides, **Lynronne 2D$_{all}$** is likely to act against *M. tuberculosis* through a potential non-membrane targeting mechanism of action.

Finally, the low hemolytic and negligible cytotoxic activities of these four **all-D** enantiomers against HaCaT (keratinocyte), HepG2 (liver), and BEAS-2B (bronchial epithelium) human cell lines (Fig. 3) are promising indicators for their potential use in the treatment of mycobacterial lung infections caused by *M. abscessus* or *M. tuberculosis* by oral administration, aerosol or nebulized inhalation. This is further illustrated by the determination of their respective Therapeutic Index (TI) (Table 4). The high TI values obtained for **Lynronne 2D$_{all}$** and **P15sD$_{all}$** clearly indicate that both peptides would represent safe candidates for the development of therapeutic applications with regards to their antibacterial activity *versus* toxicity ratio.

5. Conclusion

In this study, we have assessed the efficacy of the **all-D** enantiomers of **Lynronne 1,2** & **3**, and **P15s** AMPs from bovine rumen, against pathogenic mycobacterial infections, including infections due to *M. abscessus* and *M. tuberculosis*. We highlight the potential of the protease-resistant **Lynronne 2D$_{all}$** and **P15sD$_{all}$** which are active against all mycobacterial strains tested, and especially against both the extracellular and intracellular forms of *M. tuberculosis* H37Rv. This dual activity underscores their promise as potent scaffolds for the development of anti-TB therapeutic agents.

Notably, **Lynronne 2D$_{all}$** and **P15sD$_{all}$** achieved the highest therapeutic indexes (TI), positioning them as lead candidates for safe and effective alternatives to combat mycobacterial infections without significant toxicity or hemolytic activity to host cells. Future research, including *in vivo* studies and investigations of synergistic applications, will be essential to fully realize the therapeutic potential of these two **all-D** peptides. These findings will pave the way for the development of innovative and safer treatment strategies to address the pressing challenge of mycobacterial infections.

CRediT authorship contribution statement

Céline Boidin-Wichlacz: Conceptualization, Formal analysis, Investigation, Methodology, Validation, Visualization, Writing – review & editing. **Marc Maresca:** Conceptualization, Formal analysis, Investigation, Methodology, Validation, Visualization, Writing – review & editing. **Isabelle Correia:** Data curation, Formal analysis, Investigation, Writing – review & editing. **Olivier Lequin:** Data curation, Formal analysis, Investigation, Visualization, Writing – review & editing. **Vanessa Point:** Formal analysis, Investigation, Resources, Writing – review & editing. **Magali Casanova:** Formal analysis, Investigation, Writing – review & editing. **Alexis Reinbold:** Formal analysis, Investigation, Writing – review & editing. **Olga Iranzo:** Formal analysis, Writing – review & editing. **Sharon A. Huws:** Writing – review & editing. **Priscille Brodin:** Writing – review & editing. **Linda B. Oyama:** Writing – review & editing. **Aurélie Tasiemski:** Writing – review & editing. **Stéphane Canaan:** Conceptualization, Writing – review & editing. **Jean-François Cavalier:** Conceptualization, Formal analysis, Investigation, Methodology, Supervision, Validation, Visualization, Writing – original draft, Writing – review & editing, Project administration.

Declaration of competing interest

The authors declare that they have no known competing financial interests or personal relationships that could have appeared to influence the work reported in this paper.

Acknowledgements

This work was supported by the CNRS, Aix Marseille University and University of Lille. A.R. PhD fellowship is supported by the Ministère de l'Enseignement Supérieur et de la Recherche Française.

Supplementary materials

Supplementary material associated with this article can be found, in the online version, at doi:10.1016/j.crmicr.2025.100395.

Data availability

All data generated and analyzed during this study are included in this article and/or the **Supplementary Material**. All other relevant data are available from the authors upon reasonable request.

References

Abedinzadeh, M., Gaeini, M., Sardari, S., 2015. Natural antimicrobial peptides against mycobacterium tuberculosis. J. Antimicrob. Chemother 70 (5), 1285–1289. https://doi.org/10.1093/jac/dku570.

Ageitos, J.M., Sanchez-Perez, A., Calo-Mata, P., Villa, T.G., 2017. Antimicrobial peptides (AMPs): ancient compounds that represent novel weapons in the fight against bacteria. Biochem. Pharmacol. 133, 117–138. https://doi.org/10.1016/j.bcp.2016.09.018.

Alexander, P.J., Oyama, L.B., Olleik, H., Godoy Santos, F., O'Brien, S., Cookson, A., Cochrane, S.A., Gilmore, B.F., Maresca, M., Huws, S.A., 2024. Microbiome-derived antimicrobial peptides show therapeutic activity against the critically important priority pathogen, Acinetobacter baumannii. NPJ. Biofilms. Microbiomes. 10 (1), 92. https://doi.org/10.1038/s41522-024-00560-2.

Aubry, A., Mougari, F., Reibel, F., Cambau, E., 2017. Mycobacterium marinum. Microbiol. Spectr. 5 (2). https://doi.org/10.1128/microbiolspec.TNMI7-0038-2016.

Begg, E.J., Barclay, M.L., Kirkpatrick, C.M., 2001. The therapeutic monitoring of antimicrobial agents. Br. J. Clin. Pharmacol. 52 (Suppl 1), 35S–43S. https://doi.org/10.1046/j.1365-2125.2001.0520s1035.x.

Benarouche, A., Point, V., Parsiegla, G., Carriere, F., Cavalier, J.F., 2013. New insights into the pH-dependent interfacial adsorption of dog gastric lipase using the monolayer technique. Colloids. Surf. B Biointerfaces. 111, 306–312. https://doi.org/10.1016/j.colsurfb.2013.06.025.

Bento, C.M., Gomes, M.S., Silva, T., 2020. Looking beyond typical treatments for atypical mycobacteria. Antibiotics. (Basel) 9 (1), 18. https://doi.org/10.3390/antibiotics9010018.

Bernard, E.M., Fearns, A., Bussi, C., Santucci, P., Peddie, C.J., Lai, R.J., Collinson, L.M., Gutierrez, M.G., 2020. M. tuberculosis infection of human iPSC-derived macrophages reveals complex membrane dynamics during xenophagy evasion. J. Cell Sci. 134 (5). https://doi.org/10.1242/jcs.252973.

Blanco-Ruano, D., Roberts, D.M., Gonzalez-Del-Rio, R., Álvarez, D., Rebollo, M.J., Pérez-Herrán, E., Mendoza, A., 2015. Antimicrobial susceptibility testing for mycobacterium sp. In: Parish, T., Roberts, M.D. (Eds.), Mycobacteria Protocols. Springer New York, New York, NY, pp. 257–268.

Boisselier, E., Calvez, P., Demers, E., Cantin, L., Salesse, C., 2012. Influence of the physical state of phospholipid monolayers on protein binding. Langmuir. 28 (25), 9680–9688. https://doi.org/10.1021/la301135z.

Brodin, P., Christophe, T., 2011. High-content screening in infectious diseases. Curr. Opin. Chem. Biol. 15 (4), 534–539. https://doi.org/10.1016/j.cbpa.2011.05.023.

Broncano-Lavado, A., Senhaji-Kacha, A., Santamaria-Corral, G., Esteban, J., Garcia-Quintanilla, M., 2022. Alternatives to antibiotics against mycobacterium abscessus. Antibiotics. (Basel) 11 (10), 1322. https://doi.org/10.3390/antibiotics11101322.

Calvez, P., Bussieres, S., Eric, D., Salesse, C., 2009. Parameters modulating the maximum insertion pressure of proteins and peptides in lipid monolayers. Biochimie 91 (6), 718–733. https://doi.org/10.1016/j.biochi.2009.03.018.

Calvez, P., Demers, E., Boisselier, E., Salesse, C., 2011. Analysis of the contribution of saturated and polyunsaturated phospholipid monolayers to the binding of proteins. Langmuir. 27 (4), 1373–1379. https://doi.org/10.1021/la104097n.

Candido, P.H., Nunes Lde, S., Marques, E.A., Folescu, T.W., Coelho, F.S., de Moura, V.C., da Silva, M.G., Gomes, K.M., Lourenco, M.C., Aguiar, F.S., Chitolina, F., Armstrong, D.T., Leao, S.C., Neves, F.P., Mello, F.C., Duarte, R.S., 2014. Multidrug-resistant nontuberculous mycobacteria isolated from cystic fibrosis patients. J. Clin. Microbiol. 52 (8), 2990–2997. https://doi.org/10.1128/JCM.00549-14.

Casanova, M., Maresca, M., Poncin, I., Point, V., Olleik, H., Boidin-Wichlacz, C., Tasiemski, A., Mabrouk, K., Cavalier, J.F., Canaan, S., 2024. Promising antibacterial efficacy of arenicin peptides against the emerging opportunistic pathogen mycobacterium abscessus. J. Biomed. Sci. 31 (1), 18. https://doi.org/10.1186/s12929-024-01007-8.

Casanova, M., Olleik, H., Hdiouech, S., Roblin, C., Cavalier, J.F., Point, V., Jeannot, K., Caron, B., Perrier, J., Charriau, S., Lafond, M., Guillaneuf, Y., Canaan, S., Lefay, C., Maresca, M., 2023. Evaluation of the efficiency of random and diblock methacrylate-based amphiphilic cationic polymers against major bacterial pathogens associated

with cystic fibrosis. Antibiotics. (Basel) (1), 12. https://doi.org/10.3390/antibiotics12010120.
Catherinot, E., Clarissou, J., Etienne, G., Ripoll, F., Emile, J.F., Daffe, M., Perronne, C., Soudais, C., Gaillard, J.L., Rottman, M., 2007. Hypervirulence of a rough variant of the mycobacterium abscessus type strain. Infect. Immun. 75 (2), 1055–1058. https://doi.org/10.1128/IAI.00835-06.
Catherinot, E., Roux, A.L., Macheras, E., Hubert, D., Matmar, M., Dannhoffer, L., Chinet, T., Morand, P., Poyart, C., Heym, B., Rottman, M., Gaillard, J.L., Herrmann, J.L., 2009. Acute respiratory failure involving an R variant of mycobacterium abscessus. J. Clin. Microbiol. 47 (1), 271–274. https://doi.org/10.1128/JCM.01478-08.
Chen, X., Su, S., Yan, Y., Yin, L., Liu, L., 2023. Anti-Pseudomonas aeruginosa activity of natural antimicrobial peptides when used alone or in combination with antibiotics. Front. Microbiol. 14, 1239540. https://doi.org/10.3389/fmicb.2023.1239540.
Christophe, T., Ewann, F., Jeon, H.K., Cechetto, J., Brodin, P., 2010. High-content imaging of mycobacterium tuberculosis-infected macrophages: an *in vitro* model for tuberculosis drug discovery. Future Med. Chem. 2 (8), 1283–1293. https://doi.org/10.4155/fmc.10.223.
Christophe, T., Jackson, M., Jeon, H.K., Fenistein, D., Contreras-Dominguez, M., Kim, J., Genovesio, A., Carralot, J.P., Ewann, F., Kim, E.H., Lee, S.Y., Kang, S., Seo, M.J., Park, E.J., Skovierova, H., Pham, H., Riccardi, G., Nam, J.Y., Marsollier, L., Kempf, M., Joly-Guillou, M.L., Oh, T., Shin, W.K., No, Z., Nehrbass, U., Brosch, R., Cole, S.T., Brodin, P., 2009. High content screening identifies decaprenyl-phosphoribose 2′ epimerase as a target for intracellular antimycobacterial inhibitors. PLoS Pathog. 5 (10), e1000645. https://doi.org/10.1371/journal.ppat.1000645.
da Silva, J.L., Gupta, S., Olivier, K.N., Zelazny, A.M., 2020. Antimicrobial peptides against drug resistant mycobacterium abscessus. Res. Microbiol. 171 (5–6), 211–214. https://doi.org/10.1016/j.resmic.2020.03.001.
Dartois, V., Dick, T., 2024. Therapeutic developments for tuberculosis and nontuberculous mycobacterial lung disease. Nat. Rev. Drug Discov. 23 (5), 381–403. https://doi.org/10.1038/s41573-024-00897-5.
Deboosere, N., Belhaouane, I., Machelart, A., Hoffmann, E., Vandeputte, A., Brodin, P., 2021. High-content analysis monitoring intracellular trafficking and replication of mycobacterium tuberculosis inside host cells. Methods Mol. Biol. 2314, 649–702. https://doi.org/10.1007/978-1-0716-1460-0_29.
Degiacomi, G., Personne, Y., Mondesert, G., Ge, X., Mandava, C.S., Hartkoorn, R.C., Boldrin, F., Goel, P., Peisker, K., Benjak, A., Barrio, M.B., Ventura, M., Brown, A.C., Leblanc, V., Bauer, A., Sanyal, S., Cole, S.T., Lagrange, S., Parish, T., Manganelli, R., 2016. Micrococcin P1 - a bactericidal thiopeptide active against mycobacterium tuberculosis. Tuberculosis. (Edinb) 100, 95–101. https://doi.org/10.1016/j.tube.2016.07.011.
Flipo, M., Desroses, M., Lecat-Guillet, N., Dirie, B., Carette, X., Leroux, F., Piveteau, C., Demirkaya, F., Lens, Z., Rucktooa, P., Villeret, V., Christophe, T., Jeon, H.K., Locht, C., Brodin, P., Deprez, B., Baulard, A.R., Willand, N., 2011. Ethionamide boosters: synthesis, biological activity, and structure-activity relationships of a series of 1,2,4-oxadiazole EthR inhibitors. J. Med. Chem. 54 (8), 2994–3010. https://doi.org/10.1021/jm200076a.
Floto, R.A., Olivier, K.N., Saiman, L., Daley, C.L., Herrmann, J.L., Nick, J.A., Noone, P.G., Bilton, D., Corris, P., Gibson, R.L., Hempstead, S.E., Koetz, K., Sabadosa, K.A., Sermet-Gaudelus, I., Smyth, A.R., van Ingen, J., Wallace, R.J., Winthrop, K.L., Marshall, B.C., Haworth, C.S., Foundation, U.S.C.F., European Cystic Fibrosis, S., 2016. US Cystic Fibrosis Foundation and European Cystic Fibrosis Society consensus recommendations for the management of non-tuberculous mycobacteria in individuals with cystic fibrosis. Thorax. 71 (Suppl 1), i1–22. https://doi.org/10.1136/thoraxjnl-2015-207360.
Foo, C.S., Lupien, A., Kienle, M., Vocat, A., Benjak, A., Sommer, R., Lamprecht, D.A., Steyn, A.J.C., Pethe, K., Piton, J., Altmann, K.H., Cole, S.T., 2018. Arylvinylpiperazine amides, a new class of potent inhibitors targeting QcrB of mycobacterium tuberculosis. mBio 9 (5). https://doi.org/10.1128/mBio.01276-18 e01276-01218.
Gavrish, E., Sit, C.S., Cao, S., Kandror, O., Spoering, A., Peoples, A., Ling, L., Fetterman, A., Hughes, D., Bissell, A., Torrey, H., Akopian, T., Mueller, A., Epstein, S., Goldberg, A., Clardy, J., Lewis, K., 2014. Lassomycin, a ribosomally synthesized cyclic peptide, kills mycobacterium tuberculosis by targeting the ATP-dependent protease ClpC1P1P2. Chem. Biol. 21 (4), 509–518. https://doi.org/10.1016/j.chembiol.2014.01.014.
Gonçalves, R.M., Monges, B.E.D., Oshiro, K.G.N., Cândido, E.D.S., Pimentel, J.P.F., Franco, O.L., Cardoso, M.H., 2025. Advantages and challenges of using antimicrobial peptides in synergism with antibiotics for treating multidrug-resistant bacteria. ACS. Infect. Dis. https://doi.org/10.1021/acsinfecdis.4c00702.
Greenfield, N., Fasman, G.D., 1969. Computed circular dichroism spectra for the evaluation of protein conformation. Biochemistry 8 (10), 4108–4116. https://doi.org/10.1021/bi00838a031.
Greenfield, N.J., 2006. Using circular dichroism spectra to estimate protein secondary structure. Nat. Protoc. 1 (6), 2876–2890. https://doi.org/10.1038/nprot.2006.202.
Griffith, D.E., Aksamit, T., Brown-Elliott, B.A., Catanzaro, A., Daley, C., Gordin, F., Holland, S.M., Horsburgh, R., Huitt, G., Iademarco, M.F., Iseman, M., Olivier, K., Ruoss, S., von Reyn, C.F., Wallace Jr., R.J., Winthrop, K., Subcommittee, A.T.S.M.D., American Thoracic, S., Infectious Disease Society of, A., 2007. An official ATS/IDSA statement: diagnosis, treatment, and prevention of nontuberculous mycobacterial diseases. Am. J. Respir. Crit. Care Med. 175 (4), 367–416. https://doi.org/10.1164/rccm.200604-571ST.
Hancock, R.E., Sahl, H.G., 2006. Antimicrobial and host-defense peptides as new anti-infective therapeutic strategies. Nat. Biotechnol. 24 (12), 1551–1557. https://doi.org/10.1038/nbt1267.
Holzwarth, G., Doty, P., 1965. The ultraviolet circular dichroism of polypeptides. J. Am. Chem. Soc. 87 (2), 218–228. https://doi.org/10.1021/ja01080a015.
Iannuzo, N., Haller, Y.A., McBride, M., Mehari, S., Lainson, J.C., Diehnelt, C.W., Haydel, S.E., 2022. High-throughput screening identifies synthetic peptides with antibacterial activity against mycobacterium abscessus and serum stability. ACS. Omega 7 (27), 23967–23977. https://doi.org/10.1021/acsomega.2c02844.
Jacobo-Delgado, Y.M., Rodriguez-Carlos, A., Serrano, C.J., Rivas-Santiago, B., 2023. Mycobacterium tuberculosis cell-wall and antimicrobial peptides: a mission impossible? Front. Immunol. 14, 1194923. https://doi.org/10.3389/fimmu.2023.1194923.
Jayawant, E.S., Hutchinson, J., Gasparikova, D., Lockey, C., Prunonosa Lara, L., Guy, C., Brooks, R.L., Dixon, A.M., 2021. Molecular basis of selectivity and activity for the antimicrobial peptide Lynronne-1 informs rational design of peptide with improved activity. Chembiochem. 22 (14), 2430–2439. https://doi.org/10.1002/cbic.202100151.
Jia, F., Wang, J., Peng, J., Zhao, P., Kong, Z., Wang, K., Yan, W., Wang, R., 2017. D-amino acid substitution enhances the stability of antimicrobial peptide polybia-CP. Acta Biochim. Biophys. Sin. (Shanghai) 49 (10), 916–925. https://doi.org/10.1093/abbs/gmx091.
Johansen, M.D., Herrmann, J.L., Kremer, L., 2020. Non-tuberculous mycobacteria and the rise of mycobacterium abscessus. Nat. Rev. Microbiol. 18 (7), 392–407. https://doi.org/10.1038/s41579-020-0331-1.
Lan, Y., Lam, J.T., Siu, G.K., Yam, W.C., Mason, A.J., Lam, J.K., 2014. Cationic amphipathic D-enantiomeric antimicrobial peptides with *in vitro* and ex vivo activity against drug-resistant mycobacterium tuberculosis. Tuberculosis. (Edinb) 94 (6), 678–689. https://doi.org/10.1016/j.tube.2014.08.001.
Leung, J.M., Olivier, K.N., 2013. Nontuberculous mycobacteria in patients with cystic fibrosis. Semin. Respir. Crit. Care Med. 34 (1), 124–134. https://doi.org/10.1055/s-0033-1333574.
Li, B., Zhang, Y., Guo, Q., He, S., Fan, J., Xu, L., Zhang, Z., Wu, W., Chu, H., 2022. Antibacterial peptide RP557 increases the antibiotic sensitivity of mycobacterium abscessus by inhibiting biofilm formation. Sci. Total. Environ. 807 (Pt 3), 151855. https://doi.org/10.1016/j.scitotenv.2021.151855.
Liu, K.C., Pace, H., Larsson, E., Hossain, S., Kabedev, A., Shukla, A., Jerschabek, V., Mohan, J., Bergstrom, C.A.S., Bally, M., Schwieger, C., Hubert, M., Lundmark, R., 2022. Membrane insertion mechanism of the caveola coat protein Cavin1. Proc. Natl. Acad. Sci. U.S.A. 119 (25), e2202295119. https://doi.org/10.1073/pnas.2202295119.
Ma, X., Wang, Q., Ren, K., Xu, T., Zhang, Z., Xu, M., Rao, Z., Zhang, X., 2024. A review of antimicrobial peptides: structure, mechanism of action, and molecular optimization strategies. Fermentation 10. https://doi.org/10.3390/fermentation10110540.
Madani, A., Ridenour, J.N., Martin, B.P., Paudel, R.R., Abdul Basir, A., Le Moigne, V., Herrmann, J.L., Audebert, S., Camoin, L., Kremer, L., Spilling, C.D., Canaan, S., Cavalier, J.F., 2019. Cyclipostins and cyclophostin analogues as multitarget inhibitors that impair growth of *mycobacterium abscessus*. ACS. Infect. Dis. 5 (9), 1597–1608. https://doi.org/10.1021/acsinfecdis.9b00172.
Marsh, D., 1996. Lateral pressure in membranes. Biochim. Biophys. Acta 1286 (3), 183–223. https://doi.org/10.1016/s0304-4157(96)00009-3.
Mehta, K., Sharma, P., Mujawar, S., Vyas, A., 2022. Role of antimicrobial peptides in treatment and prevention of mycobacterium tuberculosis: a review. Int. J. Pept. Res. Ther. 28 (5), 132. https://doi.org/10.1007/s10989-022-10435-9.
Morgavi, D.P., Kelly, W.J., Janssen, P.H., Attwood, G.T., 2013. Rumen microbial (meta) genomics and its application to ruminant production. Animal. 7 (Suppl 1), 184–201. https://doi.org/10.1017/S1751731112000419.
Motta, I., Boeree, M., Chesov, D., Dheda, K., Gunther, G., Horsburgh Jr., C.R., Kherabi, Y., Lange, C., Lienhardt, C., McIlleron, H.M., Paton, N.I., Stagg, H.R., Thwaites, G., Udwadia, Z., Van Crevel, R., Velasquez, G.E., Wilkinson, R.J., Guglielmetti, L., Study group on Mycobacteria of the European Society of Clinical, M., Infectious, D., 2024. Recent advances in the treatment of tuberculosis. Clin. Microbiol. Infect. 30 (9), 1107–1114. https://doi.org/10.1016/j.cmi.2023.07.013.
Mulkern, A.J., Oyama, L.B., Cookson, A.R., Creevey, C.J., Wilkinson, T.J., Olleik, H., Maresca, M., da Silva, G.C., Fontes, P.P., Bazzolli, D.M.S., Mantovani, H.C., Damaris, B.F., Mur, L.A.J., Huws, S.A., 2022. Microbiome-derived antimicrobial peptides offer therapeutic solutions for the treatment of Pseudomonas aeruginosa infections. NPJ. Biofilms. Microbiomes. 8 (1), 70. https://doi.org/10.1038/s41522-022-00332-w.
Nessar, R., Cambau, E., Reyrat, J.M., Murray, A., Gicquel, B., 2012. Mycobacterium abscessus: a new antibiotic nightmare. J. Antimicrob. Chemother. 67 (4), 810–818. https://doi.org/10.1093/jac/dkr578.
Nguyen, P.C., Delorme, V., Bénarouche, A., Guy, A., Landry, V., Audebert, S., Pophillat, M., Camoin, L., Crauste, C., Galano, J.-M., Durand, T., Brodin, P., Canaan, S., Cavalier, J.-F., 2018. Oxadiazolone derivatives, new promising multi-target inhibitors against M. tuberculosis. Bioorg. Chem. 81, 414–424. https://doi.org/10.1016/j.bioorg.2018.08.025.
Nguyen, P.C., Delorme, V., Bénarouche, A., Martin, B.P., Paudel, R., Gnawali, G.R., Madani, A., Puppo, R., Landry, V., Kremer, L., Brodin, P., Spilling, C.D., Cavalier, J.-F., Canaan, S., 2017. Cyclipostins and cyclophostin analogs as promising compounds in the fight against tuberculosis. Sci. Rep. 7 (1), 11751. https://doi.org/10.1038/s41598-017-11843-4.
Onime, L.A., Oyama, L.B., Thomas, B.J., Gani, J., Alexander, P., Waddams, K.E., Cookson, A., Fernandez-Fuentes, N., Creevey, C.J., Huws, S.A., 2021. The rumen eukaryotome is a source of novel antimicrobial peptides with therapeutic potential. BMC. Microbiol. 21 (1), 105. https://doi.org/10.1186/s12866-021-02172-8.
Oyama, L.B., Girdwood, S.E., Cookson, A.R., Fernandez-Fuentes, N., Prive, F., Vallin, H. E., Wilkinson, T.J., Golyshin, P.N., Golyshina, O.V., Mikut, R., Hilpert, K., Richards, J., Wootton, M., Edwards, J.E., Maresca, M., Perrier, J., Lundy, F.T.,

Luo, Y., Zhou, M., Hess, M., Mantovani, H.C., Creevey, C.J., Huws, S.A., 2017. The rumen microbiome: an underexplored resource for novel antimicrobial discovery. NPJ. Biofilms. Microbiomes. 3, 33. https://doi.org/10.1038/s41522-017-0042-1.

Oyama, L.B., Olleik, H., Teixeira, A.C.N., Guidini, M.M., Pickup, J.A., Hui, B.Y.P., Vidal, N., Cookson, A.R., Vallin, H., Wilkinson, T., Bazzolli, D.M.S., Richards, J., Wootton, M., Mikut, R., Hilpert, K., Maresca, M., Perrier, J., Hess, M., Mantovani, H. C., Fernandez-Fuentes, N., Creevey, C.J., Huws, S.A., 2022. In silico identification of two peptides with antibacterial activity against multidrug-resistant Staphylococcus aureus. NPJ. Biofilms. Microbiomes. 8 (1), 58. https://doi.org/10.1038/s41522-022-00320-0.

Palomino, J.C., Martin, A., Camacho, M., Guerra, H., Swings, J., Portaels, F., 2002. Resazurin microtiter assay plate: simple and inexpensive method for detection of drug resistance in mycobacterium tuberculosis. Antimicrob. Agents Chemother. 46 (8), 2720–2722. https://doi.org/10.1128/AAC.46.8.2720-2722.2002.

Park, J., Cho, J., Lee, C.H., Han, S.K., Yim, J.J., 2017. Progression and treatment outcomes of lung disease caused by mycobacterium abscessus and mycobacterium massiliense. Clin. Infect. Dis. 64 (3), 301–308. https://doi.org/10.1093/cid/ciw723.

Pethe, K., Bifani, P., Jang, J., Kang, S., Park, S., Ahn, S., Jiricek, J., Jung, J., Jeon, H.K., Cechetto, J., Christophe, T., Lee, H., Kempf, M., Jackson, M., Lenaerts, A.J., Pham, H., Jones, V., Seo, M.J., Kim, Y.M., Seo, M., Seo, J.J., Park, D., Ko, Y., Choi, I., Kim, R., Kim, S.Y., Lim, S., Yim, S.-A., Nam, J., Kang, H., Kwon, H., Oh, C.-T., Cho, Y., Jang, Y., Kim, J., Chua, A., Tan, B.H., Nanjundappa, M.B., Rao, S.P.S., Barnes, W.S., Wintjens, R., Walker, J.R., Alonso, S., Lee, S., Kim, J., Oh, S., Oh, T., Nehrbass, U., Han, S.-J., No, Z., Lee, J., Brodin, P., Cho, S.-N., Nam, K., Kim, J., 2013. Discovery of Q203, a potent clinical candidate for the treatment of tuberculosis. Nat. Med. 19 (9), 1157–1160. https://doi.org/10.1038/nm.3262.

Queval, C.J., Song, O.R., Deboosere, N., Delorme, V., Debrie, A.S., Iantomasi, R., Veyron-Churlet, R., Jouny, S., Redhage, K., Deloison, G., Baulard, A., Chamaillard, M., Locht, C., Brodin, P., 2016. STAT3 Represses nitric oxide synthesis in Human macrophages upon Mycobacterium tuberculosis infection. Sci. Rep. 6, 29297. https://doi.org/10.1038/srep29297.

Rao, K.U., Henderson, D.I., Krishnan, N., Puthia, M., Glegola-Madejska, I., Brive, L., Bjarnemark, F., Millqvist Fureby, A., Hjort, K., Andersson, D.I., Tenland, E., Sturegard, E., Robertson, B.D., Godaly, G., 2021. A broad spectrum anti-bacterial peptide with an adjunct potential for tuberculosis chemotherapy. Sci. Rep. 11 (1), 4201. https://doi.org/10.1038/s41598-021-83755-3.

Recchia, D., Stelitano, G., Stamilla, A., Gutierrez, D.L., Degiacomi, G., Chiarelli, L.R., Pasca, M.R., 2023. Mycobacterium abscessus infections in cystic fibrosis individuals: a review on therapeutic options. Int. J. Mol. Sci. 24 (5), 4635. https://doi.org/10.3390/ijms24054635.

Rivas-Santiago, B., Rivas Santiago, C.E., Castaneda-Delgado, J.E., Leon-Contreras, J.C., Hancock, R.E., Hernandez-Pando, R., 2013. Activity of LL-37, CRAMP and antimicrobial peptide-derived compounds E2, E6 and CP26 against mycobacterium tuberculosis. Int. J. Antimicrob. Agents 41 (2), 143–148. https://doi.org/10.1016/j.ijantimicag.2012.09.015.

Roblin, C., Chiumento, S., Bornet, O., Nouailler, M., Muller, C.S., Jeannot, K., Basset, C., Kieffer-Jaquinod, S., Coute, Y., Torelli, S., Le Pape, L., Schunemann, V., Olleik, H., De La Villeon, B., Sockeel, P., Di Pasquale, E., Nicoletti, C., Vidal, N., Poljak, L., Iranzo, O., Giardina, T., Fons, M., Devillard, E., Polard, P., Maresca, M., Perrier, J., Atta, M., Guerlesquin, F., Lafond, M., Duarte, V., 2020. The unusual structure of ruminococcin C1 antimicrobial peptide confers clinical properties. Proc. Natl. Acad. Sci. U.S.A. 117 (32), 19168–19177. https://doi.org/10.1073/pnas.2004045117.

Sambandamurthy, V.K., Derrick, S.C., Hsu, T., Chen, B., Larsen, M.H., Jalapathy, K.V., Chen, M., Kim, J., Porcelli, S.A., Chan, J., Morris, S.L., Jacobs Jr., W.R., 2006. Mycobacterium tuberculosis DeltaRD1 DeltapanCD: a safe and limited replicating mutant strain that protects immunocompetent and immunocompromised mice against experimental tuberculosis. Vaccine 24 (37–39), 6309–6320. https://doi.org/10.1016/j.vaccine.2006.05.097.

Saxena, S., Spaink, H.P., Forn-Cuní, G., 2021. Drug resistance in nontuberculous mycobacteria: mechanisms and models. Biology 10 (2). https://doi.org/10.3390/biology10020096.

Shen, Y., Maupetit, J., Derreumaux, P., Tuffery, P., 2014. Improved PEP-FOLD approach for peptide and miniprotein structure prediction. J. Chem. Theory. Comput. 10 (10), 4745–4758. https://doi.org/10.1021/ct500592m.

Stout, J.E., Koh, W.J., Yew, W.W., 2016. Update on pulmonary disease due to non-tuberculous mycobacteria. Int. J. Infect. Dis. 45, 123–134. https://doi.org/10.1016/j.ijid.2016.03.006.

Sudadech, P., Roytrakul, S., Kaewprasert, O., Sirichoat, A., Chetchotisakd, P., Kanthawong, S., Faksri, K., 2021. Assessment of *in vitro* activities of novel modified antimicrobial peptides against clarithromycin resistant mycobacterium abscessus. PLoS. One 16 (11), e0260003. https://doi.org/10.1371/journal.pone.0260003.

Tamargo, J., Le Heuzey, J.Y., Mabo, P., 2015. Narrow therapeutic index drugs: a clinical pharmacological consideration to flecainide. Eur. J. Clin. Pharmacol. 71 (5), 549–567. https://doi.org/10.1007/s00228-015-1832-0.

Thevenet, P., Shen, Y., Maupetit, J., Guyon, F., Derreumaux, P., Tuffery, P., 2012. PEP-FOLD: an updated de novo structure prediction server for both linear and disulfide bonded cyclic peptides. Nucleic. Acids. Res. 40, W288–W293. https://doi.org/10.1093/nar/gks419.

Venyaminov, S., Baikalov, I.A., Shen, Z.M., Wu, C.S., Yang, J.T., 1993. Circular dichroic analysis of denatured proteins: inclusion of denatured proteins in the reference set. Anal. Biochem. 214 (1), 17–24. https://doi.org/10.1006/abio.1993.1450.

Whitmore, L., Wallace, B.A., 2004. DICHROWEB, an online server for protein secondary structure analyses from circular dichroism spectroscopic data. Nucleic. Acids. Res. 32 (Web Server issue), W668–W673. https://doi.org/10.1093/nar/gkh371.

WHO, 2024a. Global tuberculosis report. https://www.who.int/teams/global-tuberculosis-programme/data.

WHO, 2024b. WHO bacterial priority pathogens list, 2024: bacterial pathogens of public health importance to guide research, development and strategies to prevent and control antimicrobial resistance. Retrieved 19 December 2024, from. https://www.who.int/publications/i/item/9789240093461.

Wimley, W.C., Hristova, K., 2011. Antimicrobial peptides: successes, challenges and unanswered questions. J. Membr. Biol. 239 (1–2), 27–34. https://doi.org/10.1007/s00232-011-9343-0.

Woods, G.L., Brown-Elliott, B.A., Conville, P.S., Desmond, E.P., Hall, G.S., Lin, G., Pfyffer, G.E., Ridderhof, J.C., Siddiqi, S.H., Wallace, R.J., Warren, N.G., Witebsky, F. G., 2011. Susceptibility Testing of Mycobacteria, Nocardiae, and Other Aerobic Actinomycetes, 2nd Ed. Clinical and Laboratory Standards Institute, Wayne (PA).

Zanetti, M., 2004. Cathelicidins, multifunctional peptides of the innate immunity. J. Leukoc. Biol. 75 (1), 39–48. https://doi.org/10.1189/jlb.0403147.

Zhu, J., Liu, Y.J., Fortune, S.M., 2023. Spatiotemporal perspectives on tuberculosis chemotherapy. Curr. Opin. Microbiol. 72, 102266. https://doi.org/10.1016/j.mib.2023.102266.